#71

NASA CR-54882
PWA-2698

FIRST QUARTERLY REPORT
VAPOR-CHAMBER FIN STUDIES

prepared for
National Aeronautics and Space Administration

September 1965

Contract NAS3-7622

Technical Management
NASA Lewis Research Center
Space Power System Division
Nuclear Power Technology Branch
Cleveland, Ohio
Martin Gutstein

Written by L. Langston — L. Langston, Asst. Proj. Eng.

H. R. Kunz — H. R. Kunz, Program Manager

Approved by W. J. Lueckel — W. J. Lueckel, Chief, Space Power Systems

Pratt & Whitney Aircraft DIVISION OF UNITED AIRCRAFT CORPORATION

EAST HARTFORD • CONNECTICUT

FOREWORD

This report describes the progress of work conducted between May 28 and August 28, 1965 by the Pratt & Whitney Aircraft Division of United Aircraft Corporation, East Hartford, Connecticut on Contract NAS3-7622, Vapor-Chamber Fin Studies, for the Lewis Research Center of the National Aeronautics and Space Administration.

The work reported was conducted by J. Barnes, D. Patterson, A. Sherman, and the authors.

TABLE OF CONTENTS

LIST OF FIGURES

LIST OF FIGURES (Continued)

16569

I. SUMMARY

This report describes the work completed during the first three months of an experimental and theoretical program formulated for obtaining an understanding of the operation of vapor-chamber fins. Results of this program should enable the application of this device to various proposed uses.

A mechanistic model and a simplified analysis of fin operation are derived. This model indicates that experimental data is necessary on the permeability, capillary rise, and boiling in fin wicks before an understanding of fin operation can be obtained. Experiments are therefore defined to obtain these quantities. Permeability will be determined by measuring the pressure drop as a function of liquid flow rate through wick specimens. Capillary rise will be determined by measuring the maximum static height that a liquid will rise in a wick. Boiling tests will determine the maximum heat flux density that can be added to liquid-filled wicks before film-boiling occurs. Descriptions of the experimental apparatus to be used in each of these tests are presented. The manner in which the results from these tests will be used to define fin operating characteristics is indicated.

Author

II. INTRODUCTION

The work of Grover, et al[1], and other investigators[2, 3] has shown that the heat pipe is a heat transfer device that can exhibit an extremely high effective thermal conductivity, much greater in fact than any known homogeneous material. The heat pipe consists of a long closed container in which vaporization and condensation of a fluid take place. Heat added at one end of the container causes evaporation of liquid into vapor. Condensation of the vapor along the length of the container maintains the surface at a nearly constant temperature. The resulting condensate is returned to the heated end of the container by the action of capillary forces in the liquid layer which is contained in a wick lining the inside of the cavity.

A parametric study done by Haller, Lieblein, and Lindow[4] indicates that the heat pipe might be used as a "vapor-chamber fin" in reducing the weight of a radiator for a Rankine-cycle space powerplant. Such a fin is shown in cross-section in Figure 1. Two possible vapor-chamber fin configurations for use in a space radiator are shown in Figure 2.

The purpose of the present study is to explore and define the mechanism of heat transport in the vapor-chamber fin, so that a more complete evaluation can be made of its applicability to radiators for space powerplants and other uses. The program is divided into four parts, 1) wicking studies, 2) boiling studies, 3) steady-state fin operation, and 4) transient fin operation.

In order to obtain an understanding of fin operation, the wicking and boiling studies must be conducted in order to evaluate the capillary and frictional forces associated with the wicking materials, and the boiling heat transfer characteristics of wicks to be used in the fin. The mechanistic model and simplified analysis of fin operation presented in Section III of this report indicates the need for this information. Section IV lists and explains the selection of wicking materials and fin fluids to be tested. The wicking material studies are treated in Section V, where an explanation and description of the equations and experimental apparatus necessary to evaluate the forces acting on a liquid flowing in a wick are given. The test program required to measure the boiling and evaporation heat transfer properties of a liquid in a wicking material is discussed in Section VI.

[1] See Appendix 1 for numbered references

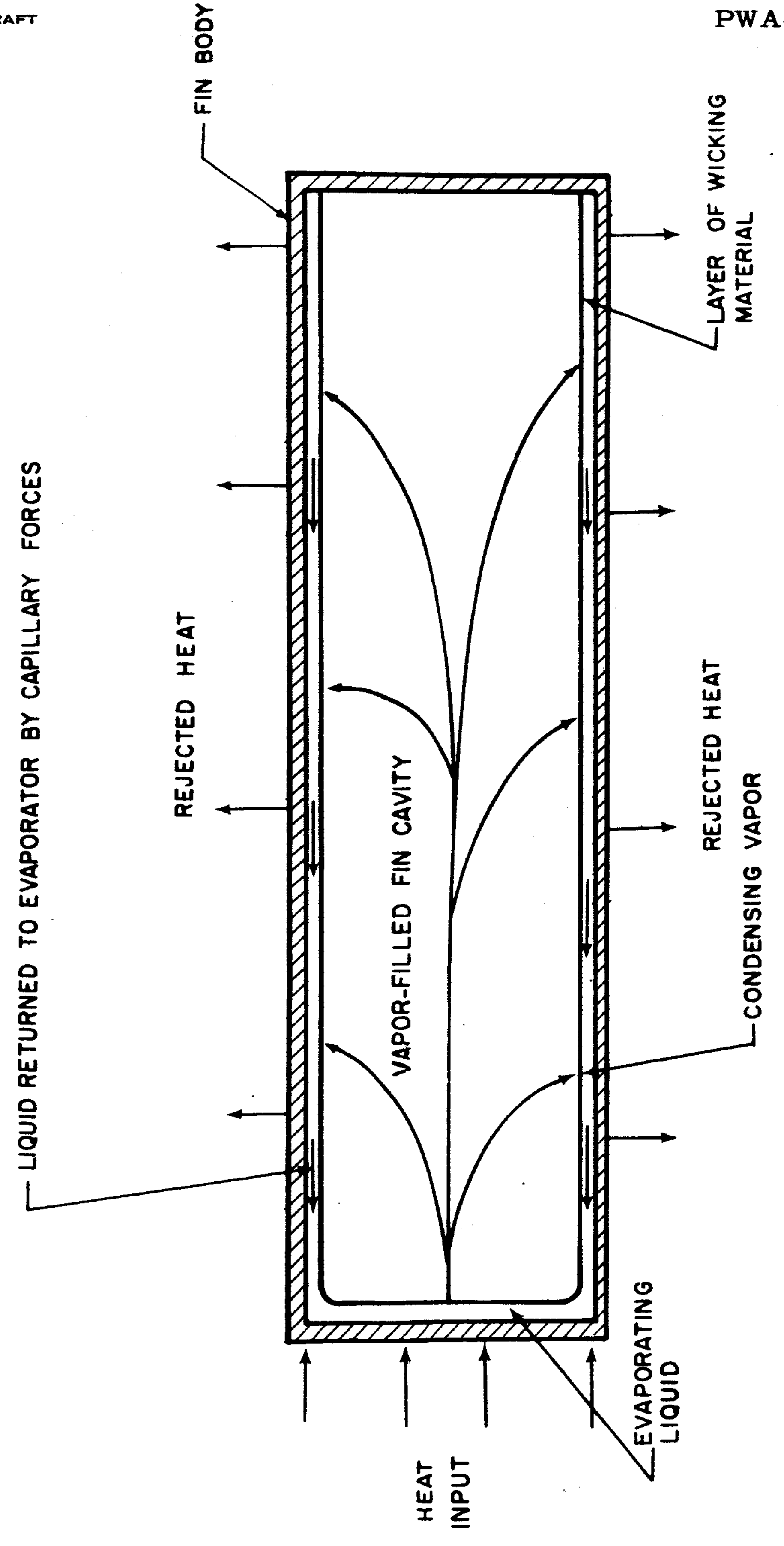

Figure 1 Vapor-Chamber Fin in Operation

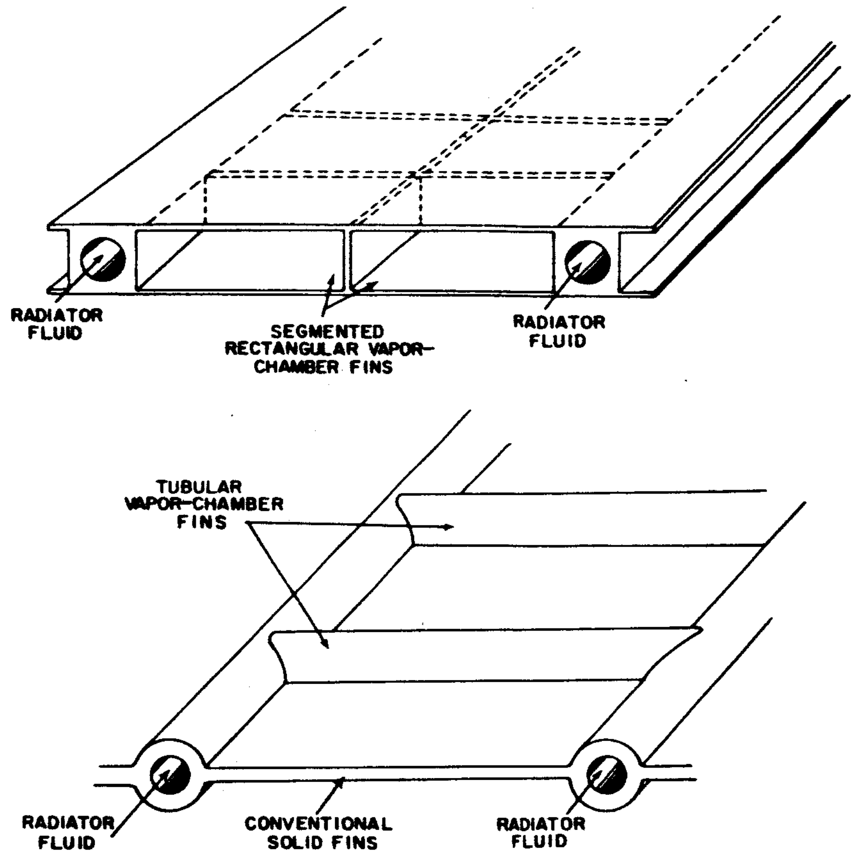

Figure 2 Two Vapor-Chamber Fin Geometries for Use on Space Radiators, Box Geometry and Tubular Geometry

After an understanding of wicking and boiling characteristics of wicking materials is obtained in these two studies, actual fins will be constructed and evaluated in steady-state and transient operation. These tests will enable an evaluation of the analytical model of the fin which has been formulated. Changes in the assumed model will be made as required to bring the model into agreement with the actual fin operation. It is hoped a technique will thereby be developed for predicting the performance of the vapor-chamber fin in other applications.

This report deals with the work completed during the first three months of the contract. Section VII discusses the work to be accomplished during the next quarter.

III. ANALYSIS OF VAPOR-CHAMBER FIN

A. Vapor-Chamber Fin Operation

The various mechanisms that control the operation of the vapor-chamber fin can best be discussed by considering the schematic diagram of the fin shown in Figure 3. This diagram illustrates the fact that the vapor-chamber fin is similar to a heat engine consisting of an evaporator, a condenser, and a pump. Although there is no net work output, pumping work is provided by capillary forces in transporting the liquid from the condenser to the evaporator.

In the evaporator section of the fin, heat must be conducted from the source of heat through the metal wall of the fin and the composite layer of liquid and wicking material in contact with the wall. This energy transfer results in evaporation of the liquid at the liquid-vapor interface.

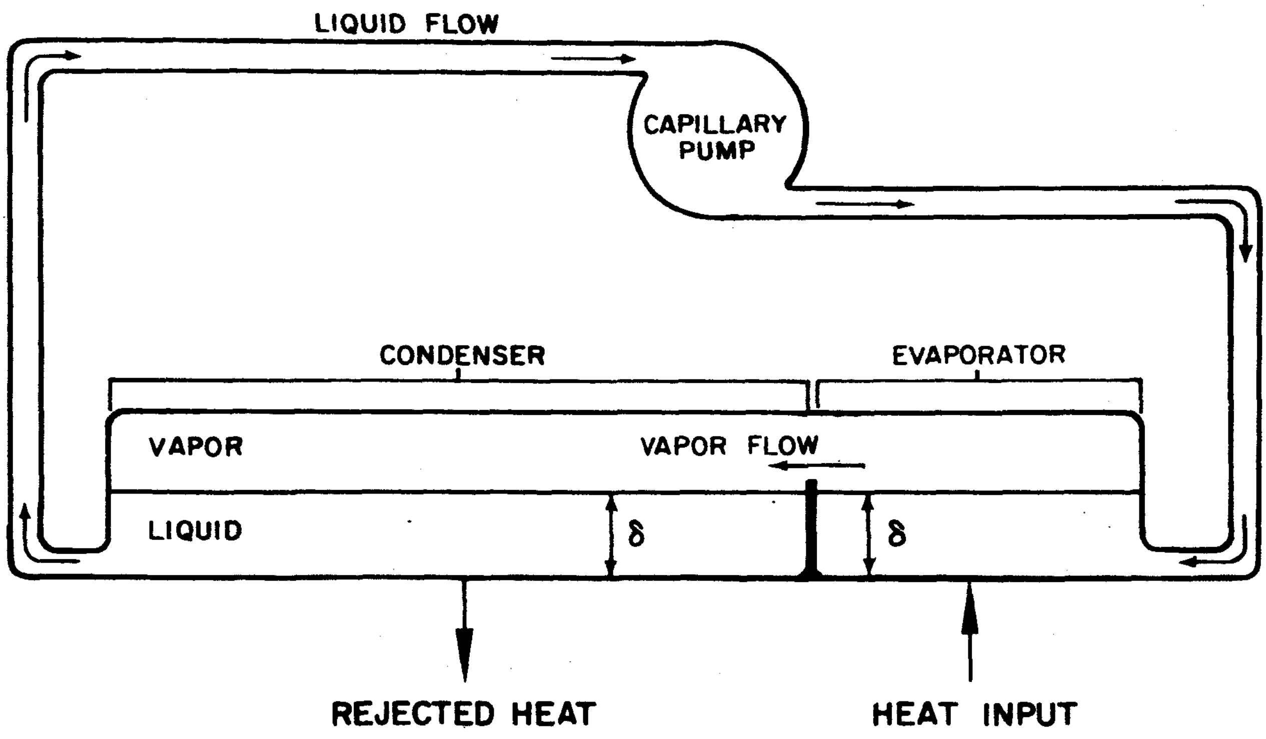

Figure 3 Mechanistic Model of Vapor-Chamber Fin

In the condenser section of the fin the reverse process to that in the evaporator occurs. Vapor condenses at the liquid-vapor interface, liberating its latent heat of vaporization. This energy is then conducted through the composite liquid-wick layer to the fin wall, then through the fin wall itself, from which it is rejected to the environment of the fin. Radiation is the mode of heat rejection from the fin in a space-radiator application.

The capillary pump serves the function of returning the condensed liquid to the evaporator. The pump may consist of a wicking material, the pores of which are small enough to provide capillary forces of sufficient magnitude to cause the liquid to flow back to the evaporator. The differences in the radius of curvature of the liquid-vapor interface in the condensing and evaporating sections of the fin provide the driving force of the pump. The details of this capillary pumping will be discussed in some detail in Section III. C. below.

When the various transport processes that occur during fin operation are analyzed, it is found that there are essentially two phenomena that limit the maximum rate of energy that the fin can transfer. They are:

1) The heat flux at which apparent film-boilingoccurs in the wick of the evaporator, and

2) The maximum liquid flow rate that the capillary pump can provide to the evaporator.

There may be other limiting phenomena, depending on the particular application in which the fin is used. For example, the thermal conductivity of the liquid-wick layer may be of such a magnitude as to provide a significant resistance to heat flow. But for the present study in which conventional liquids and space-radiator geometries will be studied, the film-boiling heat flux and the maximum capillary pump output seem to be the two limitations of most importance. Thus, although other factors that influence the operation of the fin will be taken into account in this program, these two phenomena will be studied separately and in greater detail.

It is unfortunate that these two limiting phenomena depend on the wick; for in the near-zero gravity environment of a space radiator, it is conceivable that a vapor-chamber fin wick would not be needed. The liquid would simply wet the walls of the fin cavity and due to changes in the radius of curvature at the liquid-vapor interface, would flow back to the evaporator section of the fin. In the present study all tests will be run in a 1-g environment, thereby necessitating the use of a wicking material in any fin models tested in order to make the capillary forces large relative to the gravitational force. However, even in an actual vapor-chamber fin space radiator, a wick of some form would probably be used to ensure that the radiator would work in a force field such as gravity. In all discussions that follow it is assumed that the fin is in a gravitational field.

When either of these limiting phenomena occurs, the result should be the same: any attempt to increase the net heat input to the fin would result in a large temperature rise at the base of the fin. This temperature increase, shown in the plot of Figure 4, is probably caused by an insufficiency of liquid at the liquid-wick-solid interface in the evaporator of the fin.

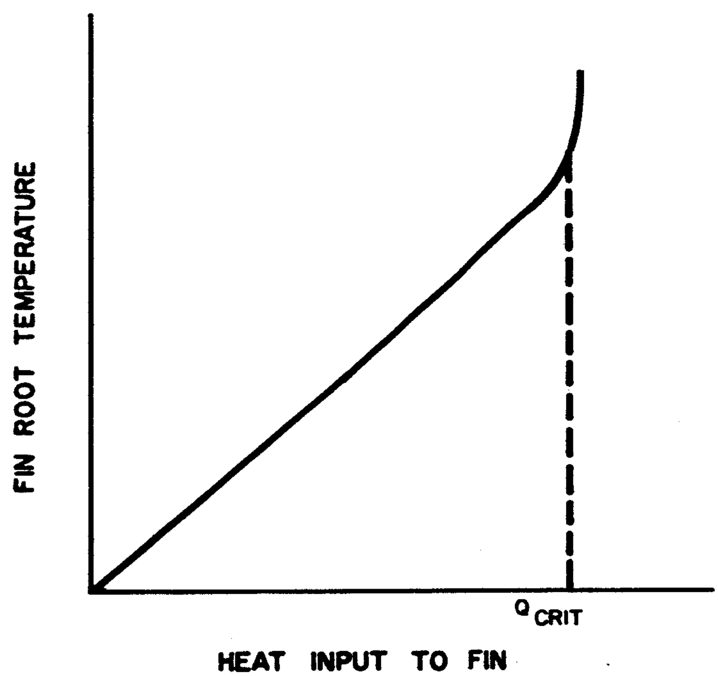

Figure 4 Performance of Vapor-Chamber Fin as Function of Heat Input for Given Test Configuration

Thus, when the performance of a vapor-chamber fin falls off as the heat input is increased, the question arises as to which of the two limiting phenomena is responsible, wick film-boiling or insufficient capillary pump output. In order to answer the question a separate evaluation of each of these two possible causes of fin failure is needed. The following two sections discuss each possibility.

B. Limitation Due to Wick Boiling

An evaluation of the first of the limiting phenomena listed in the preceding section involves a study of the process of evaporation and boiling of a liquid in a wick.

The actual process occurring in the evaporator section of the fin can be visualized in the following manner. As heat is initially added in the evaporation region, the heat will be conducted through the fin wall and the wick-liquid composite to the liquid-vapor interface where evaporation will take place. As the heat input to an operating fin is increased, the liquid-wick-solid interface temperature will rise to the point where the adjacent liquid is sufficiently superheated to cause nucleate boiling at the interface. If an equilibrium condition is to occur without excessive superheat, the capillary and/or buoyancy forces must be great enough to cause convection of the resulting vapor bubbles through the wick to the vapor cavity of the fin and supply fresh liquid to the heating surface at a sufficient rate. The buoyancy forces will be dependent upon the gravitational field in which the fin is operating. If vapor does not leave the interface at the rate at which it is produced, liquid will be excluded from the interface, causing superheated conditions and film-boiling to set in. The effects of such a process are shown in Figure 4 as a sharp increase in temperature at the base of the fin, causing the fin to eventually become ineffective.

Because of the limited success with theoretical models of the simpler case of pool boiling, an attempt to evaluate boiling heat flux limits analytically in a relatively complicated wick structure appears unpromising. Thus, an experimental program to study boiling in wicks is being conducted and will be described in Section V.

C. Limitation Due to Capillary Pump

The second major limitation on fin operation is the maximum output of the capillary pump. Stated differently, it is a matter of the wicking capability of the wick material.

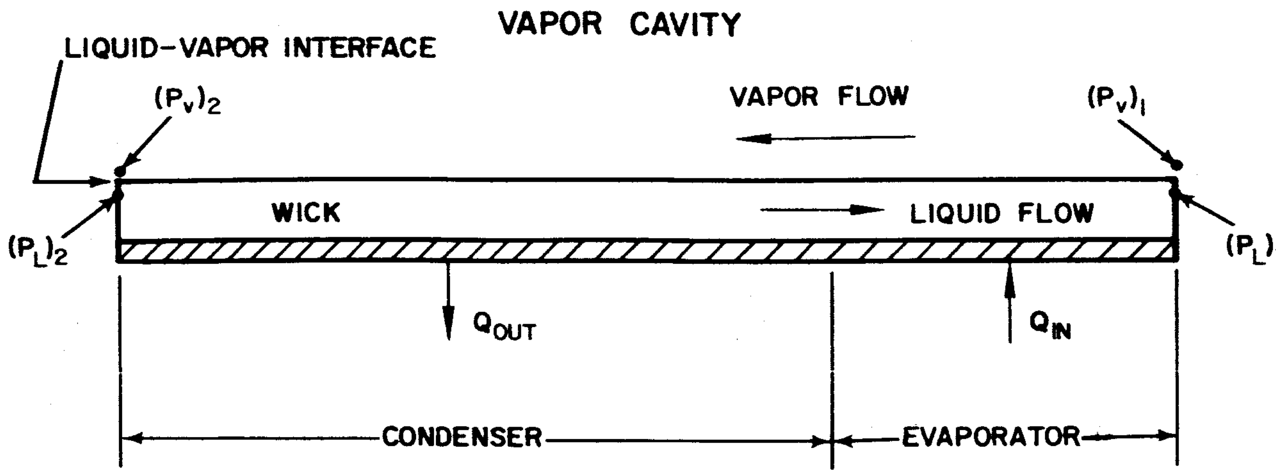

Figure 5 Two-Dimensional Model of Vapor-Chamber Fin

To analyze the action of the wick as a capillary pump, the simplified model of the vapor-chamber fin shown in Figure 5 can be considered. The liquid pressures at the ends of the fin are $(P_L)_1$ and $(P_L)_2$, while the vapor pressures at the ends directly above the liquid are $(P_V)_1$ and $(P_V)_2$ respectively. In all of the following discussions it is assumed that no boiling takes place.

For the fin to operate, there must be a liquid flow from 2 to 1. Therefore, to overcome frictional forces and momentum changes

$$(P_L)_2 > (P_L)_1 \tag{1}$$

Similarly, since there must be a counter vapor flow from 1 to 2, so that

$$(P_V)_1 > (P_V)_2 \tag{2}$$

If the system in Figure 5 is at steady state, the sum of the pressure changes that a given fluid particle experiences as it leaves the evaporator and returns again, is zero, or

$$[(P_V)_1 - (P_V)_2] + [(P_V)_2 - (P_L)_2] + [(P_L)_2 - (P_L)_1] +$$

$$[(P_L)_1 - (P_V)_1] = 0 \tag{3}$$

As the liquid flows in the wick or the gas in the cavity, the pressure changes are balanced by frictional and inertial forces. These pressure drops due to friction, rate of change of momentum, etc., can be defined as

$$(\Delta P)_d \equiv (\Delta P_V)_d + (\Delta P_L)_d \equiv \left[(P_V)_1 - (P_V)_2\right] + \left[(P_L)_2 - (P_L)_1\right] \quad (4)$$

where, in general:

$$(\Delta P_V)_d > 0 \text{ and } (\Delta P_L)_d > 0 \quad (5)$$

These terms must be positive since they consist primarily of the frictional components.

At any vapor-liquid interface there is some radius of curvature of the resulting surface, whether it be a very small value or infinity. The Laplace-Young equation of capillarity[5] shows that there is a pressure change across an interface, given by

$$\Delta P = \sigma \left(\frac{1}{R} + \frac{1}{R'} \right) \quad (6)$$

where ΔP is the pressure difference across the surface, σ is the liquid-vapor surface tension, and R and R' are the two radii of curvature necessary to describe any three-dimensional surface. The highest pressure is always on the concave side of the interface when R and R' have identical signs. When it is not clear which is the concave side (e.g., a saddle-shaped interface) the higher pressure is on the side of the smaller radius.

If the liquid wets the wick, that is, if the contact angle is less than 90°, and if it is assumed that the condenser and evaporator vapor-liquid interfaces can each be characterized by a single radius of curvature, the remaining terms in Equation (3) become

$$\left.\begin{aligned} (P_V)_2 - (P_L)_2 &= \frac{2\sigma}{R_2} \\ (P_L)_1 - (P_V)_1 &= \frac{2\sigma}{R_1} \end{aligned}\right\} \quad (7)$$

where σ is the liquid-vapor surface tension and R_1 and R_2 are the radii of curvature describing the evaporator and condenser surfaces.

Since the fin operates at a nearly constant temperature, any temperature-dependent variation of σ can be neglected. Combining Equations (3), (4), (5) and (7) yields

$$(\Delta P)_d = \frac{2\sigma}{R_1} - \frac{2\sigma}{R_2} > 0 \qquad (8)$$

This means that

$$R_1 < R_2$$

Thus, the capillary pump, that is, the wick, overcomes the frictional and inertial forces in the vapor-chamber fin by allowing a larger radius of curvature to form in the condenser than in the evaporator. Of course, the liquid must wet the wick for this to be true.

Physically this means that vapor condensing out on the wick causes a large interfacial radius of curvature to form as the liquid tends to flood the wick. However, the heat added to the evaporator makes the vapor-liquid interface retreat into the matrix of the wick, causing a smaller interfacial radius of curvature, a radius characteristic of the size of the pores in the wick itself. These differences in radii of curvature at different locations along the wick make the porous medium of the wick act as a capillary pump.

At first it might be thought that to increase the capacity of the pump it would be best to decrease the size of the pores in the wick, thereby decreasing R_1 in Equation (8). However, this also tends to increase the frictional forces in the wick. The relationship between the capillary forces, frictional forces, and inertial forces will be derived in the next section.

The upper limit on the frictional and inertial pressure drops in both the vapor and liquid can be calculated using the above expressions. The upper limit on the pressure drop through the vapor is obtained by using Equations (4), (5) and (8) to get the inequality

$$(P_V)_1 - (P_V)_2 < 2\sigma \left(\frac{1}{R_1} - \frac{1}{R_2} \right) \qquad (9)$$

The right side is maximized when the condenser is completely flooded, that is, when $R_2 \rightarrow \infty$. Hence, for the fin to operate

$$(P_V)_1 - (P_V)_2 < \frac{2\sigma}{R_1} \qquad (10)$$

Values of the right-hand side can be obtained by considering the minimum pore size in the wick, which for most wicking materials considered yields

$$\frac{2\sigma}{R_1} \approx 10 \text{ to } 20 \text{ inches of } H_2O$$

By similar reasoning it can be shown that the maximum pressure drop in the liquid is bounded by this same value.

It has been demonstrated that the shape of the liquid-vapor interface is critical to the operation of the capillary pump. In particular, the radii of curvature in the evaporator section are most crucial, for as long as the evaporator supplies sufficient vapor and the fin is sufficiently charged with liquid, the radii of curvature in the condenser will be large, making the pump term in Equation (8) strongly dependent on R_1.

It is not apparent what the actual shape or position of the entire liquid-vapor interface is in the fin evaporator. Three possible positions are shown in Figure 6.

Certainly the situation pictured in (a), where the interface has retreated only slightly into the wick matrix, is a correct representation for lower heat-input rates (assuming that the wick has been initially saturated with liquid). However, the situation cannot be so easily visualized while the wick is providing liquid flows at higher heat-input rates, for under such conditions the liquid-vapor interface is certain to retreat further into the wick. At still higher values of heat input, the wick will no longer be able to supply sufficient liquid to be evaporated. The wick matrix will then dry and the interface could assume the position shown in (b) or (c), or be a combination of these. Whatever the interfacial position, when the maximum flow rate of the pump is exceeded the evaporator will dry and the base temperature will rise, as shown in Figure 4, causing eventual loss of fin effectiveness.

Because it is not clear what the shape and position of the evaporator liquid-vapor interface will be at high heat-input rates, it is essential that an isotropic wicking material be used in the present study of the vapor-chamber fin (the term isotropic will be clarified in Section IV A). In this way any limitation in fin operation due to the maximum flow

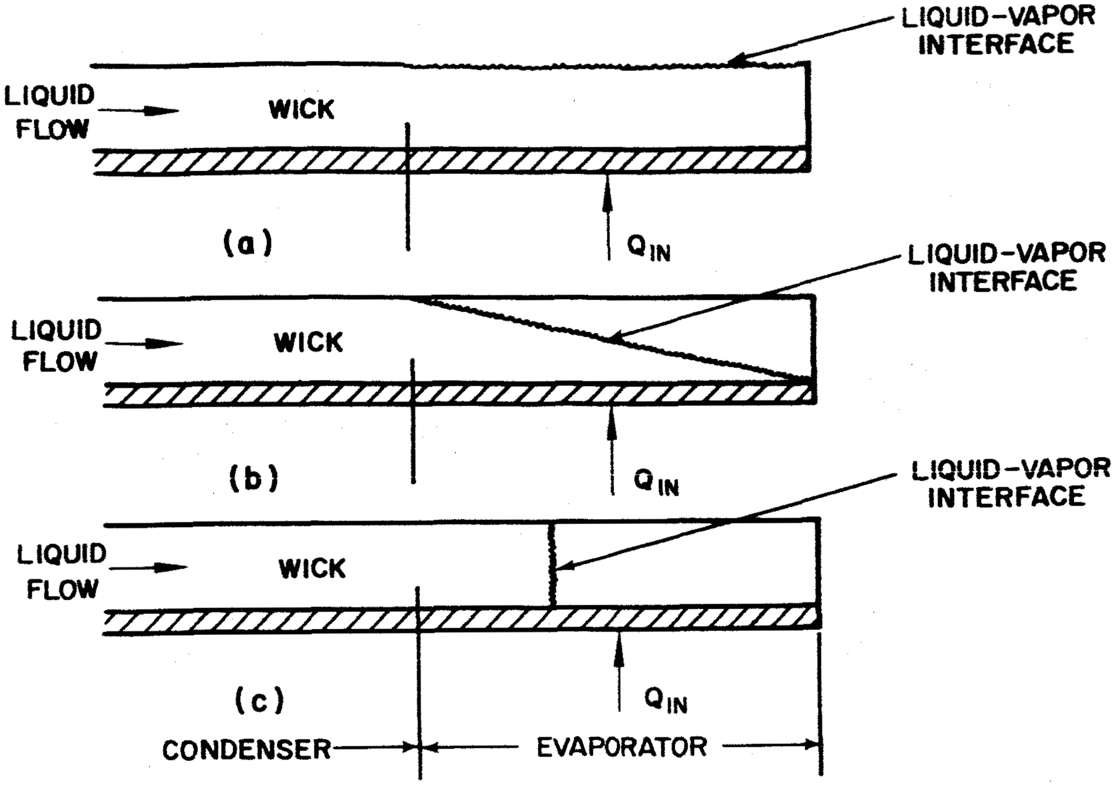

Figure 6 Simplified Picture of the Liquid-Vapor Interface in the Evaporator Section of the Fin

rate provided by the capillary pump cannot be attributed to the directional properties of the wick.

So far it has been shown how the capillary pump functions qualitatively. In the next section a simplified analytical model of the fin will be derived, based entirely on the limitations imposed by the capillary pump. The problem of wick boiling will not be treated for reasons stated in the last section. This analytic model will be of some importance for with it the relationship between the fluid and wick properties can be defined. These relationships form the basis of the wicking material studies to be carried out in the present program.

With the help of some simplifying assumptions, an expression will be derived that will show what effect the capillary pump capability has on the maximum size of a vapor-chamber fin for a given heat input, or conversely, what effect the pump has on the maximum heat input that a fin of a given size can accept.

D. Simplified Model of Vapor-Chamber Fin

This section contains the derivation of a simplified model of the vapor-chamber fin. An analytical model of the heat pipe has been formulated by Cotter[11]. The purpose of this model of the vapor-chamber fin is to discover the parameters necessary to adequately describe the mechanism of the fin. Within the framework of the assumptions made in its derivation, the model includes the effects of rate of change of momentum, surface tension forces, and the frictional forces in the body of the wicking material. The problem of wick boiling is not considered in its derivation.

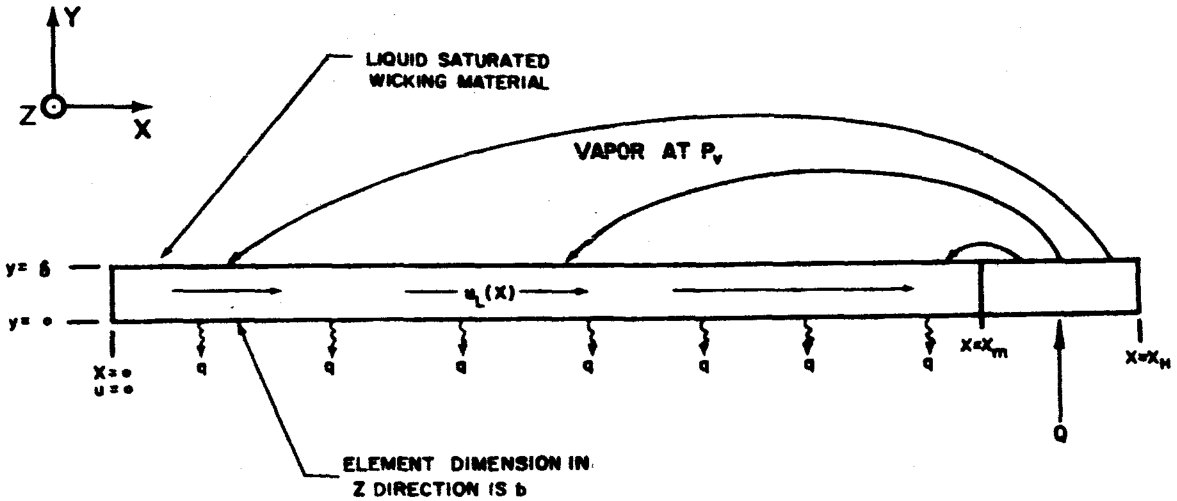

Figure 7 Simplified Model of Vapor-Chamber Fin

Figure 7 shows a simplified model of the vapor-chamber fin that is rejecting heat at a specified heat flux density q. The fin width in the z-direction is b and the heat rejecting length is x_m. Because limiting boiling heat fluxes are not being considered, the evaporator section, from $x = x_m$ to $x = x_H$, is assumed to be of sufficient size to provide enough vapor to meet the requirements set by the specified value of the condenser rejection flux density q. In addition, the following assumptions are made concerning the model shown in Figure 7:

1) The wicking material is rigid, is of constant thickness δ, and is saturated with a wetting liquid along the entire condenser length x_m.

2) The vapor and the liquid-vapor interface are at the same constant temperature from $x = 0$ to $x = x_m$. It follows that the vapor pressure P_V is also constant along this length, and that there is little conducted energy or variation in convected energy in the x or z directions within the wicking material.

3) The vapor that condenses on the liquid-vapor interface has a velocity u_V in the y-direction. This velocity has no x or z

components; thus there are no momentum contributions in these directions.

4) The effects of gravity are not considered.

5) At any given point, the liquid-vapor interface can be characterized by one radius of curvature, R.

6) The velocity of the liquid in the wicking material has an x component only, and is uniform across the wick thickness δ.

Figure 8 shows the forces and momentum fluxes associated with a differential element of the saturated wicking material at a given x in the heat rejecting portion of the fin.

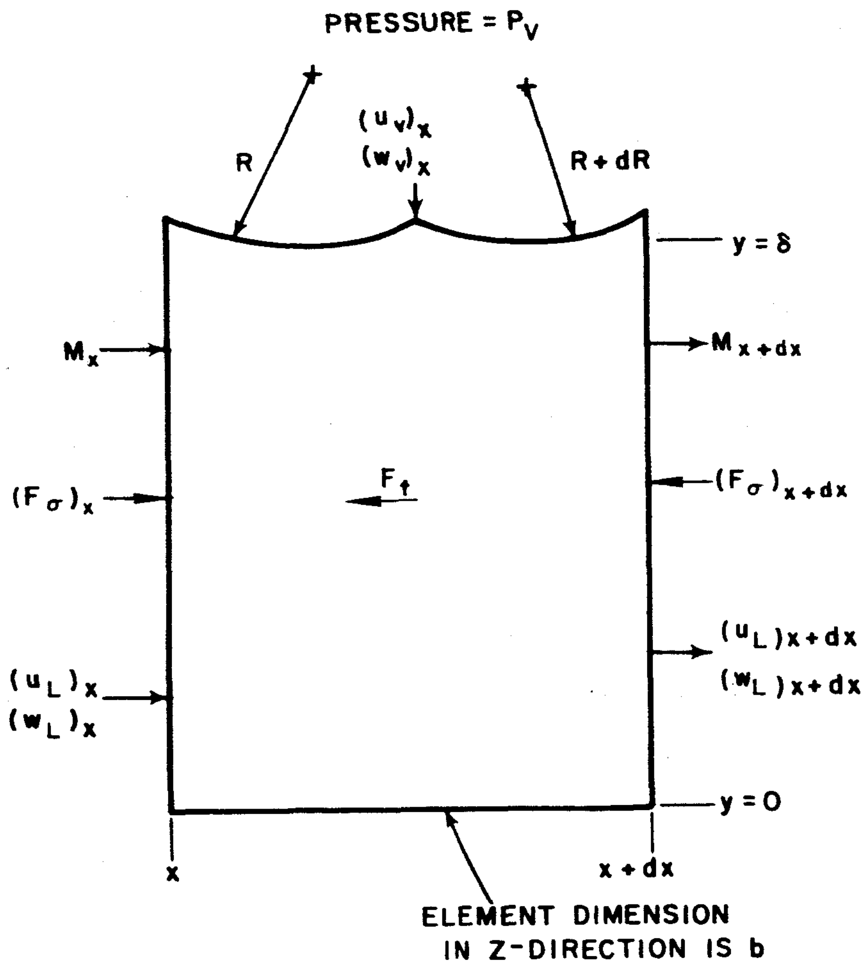

Figure 8 Differential Element of Wicking Material for Momentum Equation

Applying the continuity equation to the element of Figure 8, the relationship between the liquid flow rate w_L and the vapor flow rate w_V is obtained

$$(w_L)_x + w_V = (w_L)_{x+dx} \tag{11}$$

Because

$$(w_L)_x = \rho_L (\delta b) u_L \tag{12}$$

and

$$(w_L)_{x+dx} = \rho_L (\delta b) (u_L + \frac{du_L}{dx} dx) \tag{13}$$

where ρ_L is the liquid density. It follows that

$$w_V = \rho_L \frac{du_L}{dx} dx (\delta b) \tag{14}$$

where

$$w_V = \rho_V u_V (b dx) \tag{15}$$

and ρ_V is the vapor density.

The momentum equation in the x-direction for the element in Figure 8 is

$$F_x = M_{x+dx} - M_x \tag{16}$$

The momentum terms are

$$M_x = \frac{\rho_L}{g_o} u_L^2 (b \delta) \tag{17}$$

$$M_{x+dx} = \frac{\rho_L}{g_o} u_L^2 (b \delta) + \frac{\rho_L}{g_o} \frac{d(u_L^2)}{dx} dx (b \delta) \tag{18}$$

where g_o is the proportionality constant in Newton's second law. It should be noted that because of Assumption 3 there is no momentum contribution to Equation (16) by the vapor as it enters the top of the element. Calculations show that when such a momentum term is included, it is negligible compared to the other terms in Equation(16). In addition, the presence of the rigid wick at the liquid-vapor interface makes the inclusion of such a term doubtful.

Two forces make up the force term in Equation (16): the force of capillarity due to the differences in radius of curvature at x and x + dx, and the frictional force F_f acting on the liquid as it flows through the porous medium of the wick. Thus

$$\Sigma F_x = (F_\sigma)_x - (F_\sigma)_{x + dx} - F_f \qquad (19)$$

The capillary force F_σ is given by the Laplace-Young equation, Equation (6). Because of Assumption 5 this reduces to

$$\Delta P = \frac{2\sigma}{R} \qquad (20)$$

where ΔP is the pressure drop across the liquid-vapor interface at x, σ is the liquid-vapor surface tension, and R is the radius of curvature of the interface at x. Thus the capillary forces at x and x + dx are

$$(F_\sigma)_x = \left(P_V - \frac{2\sigma}{R} \right) (\delta b) \qquad (21)$$

$$(F_\sigma)_{x + dx} = \left(P_V - \frac{2\sigma}{R + dR} \right) (\delta b) \qquad (22)$$

where the vapor pressure P_V is constant, by Assumption 2 .

The net capillary force on the element is found by adding Equations (21) and (22) vectorially to get

$$(F_\sigma)_x - (F_\sigma)_{x + dx} = -(\delta b)(2\sigma) \frac{dR}{R^2} \qquad (23)$$

where RdR has been neglected when it is compared to R^2.

Because of the low flow rates and velocities encountered with capillary flow in wicks, the flow produced by the net capillary force in Equation (23) can be assumed to be both laminar and relatively free from inertia effects. As pointed out by Scheidegger[6], both of these conditions must be met if Darcy's law [6] for flow through porous media is to apply. Using a modified form of Darcy's law to obtain an expression for the remaining term in Equation (19) results in

$$F_f = K_1 (\delta b) \mu_L u_L dx \qquad (24)$$

where μ_L is the liquid coefficient of viscosity and K_1 is a constant of proportionality. This constant is particularly important in the evaluation of wicking materials. It is dependent on the geometry and dimensions of the passages in the wicking material and could possibly be described adequately if an equivalent passage diameter, the wick tortuosity, and porosity of the material were all known functions. Since this is usually not the case, K_1 can be determined experimentally by passing a known flow rate of liquid through the wicking material and measuring the resulting pressure drop across the sample. Then K_1, which will be called the wick friction factor, can be calculated from Equation (24). The constant K_1 has the dimensions of (length)$^{-2}$ and is the reciprocal of permeability.

Combining Equations (16), (17), (18), (23), and (24) results in the differential momentum equation

$$- 2\sigma \frac{dR}{R^2} - K_1 \mu_L u_L dx = \frac{\rho_L}{g_o} \frac{d(u_L{}^2)}{dx} dx \qquad (25)$$

The remaining relationship necessary to describe the operation of the fin is the energy equation. Figure 9 shows the energy fluxes associated with a differential wick element at some x in the condenser portion of

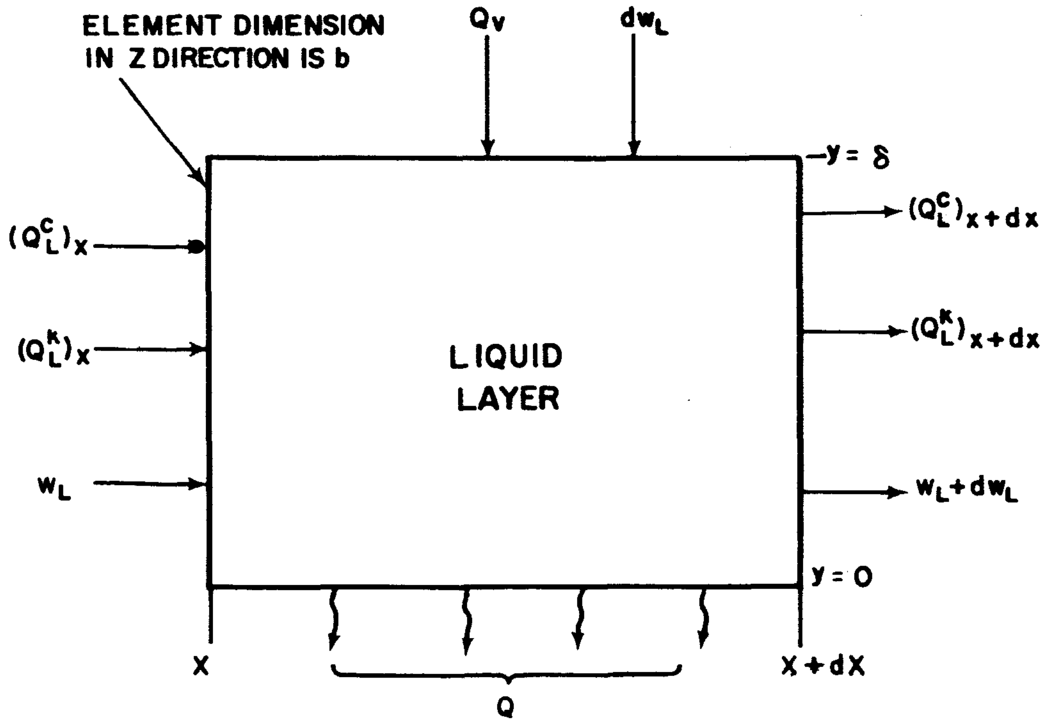

Figure 9 Differential Element of Wicking Material for Energy Equation

the fin, where Q is the energy transferred per unit time, the superscripts c and k refer to convection and conduction, and L and V refer to liquid and vapor.

Neglecting changes in kinetic energy, the individual terms in Figure 9 are given by

$$\left.\begin{array}{ll}
\underline{\text{in}} & \underline{\text{out}} \\
Q_V = Q_V^c + Q_V^k & (Q_L^c)_{x+dx} = w_L h_L + \dfrac{d(w_L h_L)}{dx}\,dx \\
(Q_L^c)_x = w_L\, h_L & (Q_L^k)_{x+dx} = -k_L\,(\delta\, b)\left[\dfrac{dT_L}{dx} + \dfrac{d^2T_L}{dx^2}\,dx\right] \\
(Q_L^k) = -k_L(\delta\, b)\dfrac{dT_L}{dx} & Q = q\,(b\ dx)
\end{array}\right\} \quad (26)$$

where h is enthalpy and k_L is the thermal conductivity of the liquid-wick combination.

Because of Assumption 2 all of the conduction terms in Equation (26) are zero. Thus the energy equation for the element in Figure 9 is

$$Q_V^c + (Q_L^c)_x = (Q_L^c)_{x+dx} + Q \qquad (27)$$

The energy entering the top surface of the element is

$$Q_V = Q_V^c = w_V\, h_V \qquad (28)$$

Combining this with the continuity equation, Equation (14) results in

$$Q_V^c = h_V\, \rho_L \frac{du_L}{dx}\, dx\ (\delta\ \ b) \qquad (29)$$

Putting Equations (29), (26), and (12) into Equation (27) yields the combined energy-continuity differential equation

$$u_L\, \rho_L \frac{dh_L}{dx} - (h_V - h_L)\, \rho_L \frac{du_L}{dx} + \frac{q}{\delta} = 0 \qquad (30)$$

But for an incompressible liquid where internal energy is a function of temperatures only, the enthalpy variation with x is expressed as

$$\frac{dh_L}{dx} = C_L\left(\frac{dT_L}{dx}\right) + \frac{1}{\rho_L}\left(\frac{dP_L}{dx}\right) \tag{31}$$

where C_L is the specific heat of the liquid. As shown in Section III. C., the pressure drop in the liquid is very small, so that

$$\frac{dP_L}{dx} \approx 0 \tag{32}$$

Also by Assumption 2

$$\frac{dT_L}{dx} = 0 \tag{33}$$

Thus

$$\frac{dh_L}{dx} \approx 0 \tag{34}$$

so that Equation (30) becomes

$$\frac{du_L}{dx} = \frac{q}{h_{VL}\delta\,\rho_L} \tag{35}$$

where h_{VL} is the latent heat of vaporization of the liquid.

Integrating Equation (35) yields the combined energy-continuity equation

$$u_L = \frac{q}{h_{VL}\delta\,\rho_L}\,x \tag{36}$$

showing that the liquid velocity varies linearly with x. The liquid flow rate then becomes

$$w_L = \frac{qb}{h_{VL}}\,x \tag{37}$$

Finally, Equations (36) and (25) can be combined to give an energy-continuity-momentum integral equation

$$- \int_{R_{x=o}}^{R_{x=x_m}} 2\sigma \frac{dR}{R^2} \quad - \int_{o}^{x_m} K_1 \frac{q}{h_{VL}\delta} \frac{\mu_L}{\rho_L} \, x \, dx = \int_{o}^{x_m} \frac{2\, q^2}{g_o \, h_{VL}^2 \, \rho_L \, \delta^2} \, x \, dx \qquad (38)$$

where, as shown in Figure 7, x_m is the length of the rejection portion of the fin.

To evaluate the maximum output of the capillary pump, Equation (37) shows that x_m must be a maximum. In Equation (38) it is seen that to maximize x_m the limits of integration on the surface tension must contain both minimum and maximum values of R. In Section III. C. it was shown that at x = 0, R can be very large and can be considered to approach an infinite value for optimum fin operation. Similarly, as shown by Equation (8) the radius of curvature in the evaporator must be at some minimum radius of curvature, R_{min}. To calculate the maximum value of x_m, the assumption is made that at

$$\left.\begin{array}{ll} & x = 0, \; R \rightarrow \infty \\ \text{and that at} & x = x_m, \; R \rightarrow R_{min} \end{array}\right\} \qquad (39)$$

where R_{min} is the minimum radius of curvature that the wicking material can support. It is further assumed that the entire evaporator liquid-vapor interface can be by characterized by R_{min}, although no assumption has to be made about the position of the interface in the evaporator.

Using the above limits for R, Equation (38) can be integrated and solved for x_m to obtain

$$x_m = \left\{ \frac{\rho_L h_{VL} \sigma}{\mu_L} \left[\frac{\dfrac{2}{R_{min}}}{\dfrac{qK_1}{2} \left(1 + \dfrac{2q}{g_o \, \mu_L \, h_{VL} \, \delta \, K_1} \right)} \right] \right\}^{1/2} \qquad (40)$$

If a range of representative values is substituted for the quantities in the non-unity term in the denominator of Equation (40), it is found that

$$\frac{2q}{g_o \mu_L h_{VL} \delta K_1} \ll 1 \qquad (41)$$

This term represents the contribution of the rate of change of liquid momentum, and can be neglected when compared to unity. Thus the expression for the maximum length of the heat rejection portion of the fin is given by

$$x_m = 2\left(\frac{\rho_L h_{VL} \sigma}{\mu_L}\right)^{1/2}\left(\frac{\delta}{K_1 q R_{min}}\right)^{1/2} \qquad (42)$$

In Equation (42) the liquid properties enter as the dimensional parameter

$$N \equiv \frac{\rho_L h_{VL} \sigma}{\mu_L} \qquad (43)$$

To maximize the performance of the fin, a liquid should have as large a value of N as possible. N for conventional liquids ranges roughly from 1 to 150 Btu hr $lb_f/ft^3\ lb_m$. By way of contrast, the liquid metal lithium has a value of N = 7950 Btu hr $lb_f/ft^3\ lb_m$ at 1500 °F.

The only quantity in Equation (42) that is not readily measurable is R_{min}. Because a maximum value of x_m is desired, R_{min} is assumed to be the smallest radius of curvature that the wick can support. One of the simplest methods of determining an effective minimum radius of curvature in a wicking material is to observe the maximum height to which the liquid rises in a vertical sample of the wicking material. If the finest pores in the vertical wick through which the liquid rises can be thought of as single capillary tubes of an equivalent diameter, the effective minimum radius of curvature is

$$R_{min} = \frac{2 g_o \sigma}{\rho_L g \ell_m} \qquad (44)$$

where ℓ_m is the maximum height of the liquid in the vertical wick when exposed to a 1-g gravity field. Equation (44) is obtained from a static force balance on the liquid in a capillary tube that has an equivalent diameter equal to the smallest wick pores. R_{min} in Equation (44) is termed the effective minimum radius of curvature because in actuality the smallest pores in a wicking material are not single capillaries but are interconnected with pores of larger size. However, Equation (44) should still be an effective measure of R_{min} for a vapor-chamber fin application. This will be demonstrated in Section V. F.

By combining Equations (44) and (42) it is seen that the final expression for the maximum length of the condenser section of the fin is given by

$$x_m = \left[\frac{2g \, \rho_L^2 \, h_{VL} \, \delta \, \ell_m}{g_o \, K_1 \, \mu_L \, q} \right]^{\frac{1}{2}} \tag{45}$$

where

g = acceleration of gravity
ρ_L = liquid density
h_{VL} = liquid latent heat of vaporization
δ = liquid wick thickness (constant)
ℓ_m = static wicking height
g_o = Newton's proportionality constant
K_1 = wick friction factor
μ_L = liquid viscosity
q = specified rate of heat rejection flux density

Thus, x_m is maximized when the wicking parameter ℓ_m/K_1 is large. It should be emphasized that gravity effects have not been considered in Equation (45) and that g, the acceleration of gravity, enters only through the separate process of determining R_{min} from Equation (44).

Equation (45) can be expressed in terms of the total fin heat input Q_T. Thus, instead of solving for x_m and specifying a heat rejection flux q, the problem can be restated to get

$$Q_T = \frac{2 g \, \rho_L^2 \, h_{VL} \, \delta \, \ell_m}{g_o \, K_1 \, \mu_L} \quad \frac{b}{x_m} \tag{46}$$

where b is the fin width in the y-direction. This is the maximum total heat input that can be transferred to a vapor-chamber fin with a condenser of length x_m.

A plot of Equation (45) is shown in Figure 10 for water at 70°F. This plot shows the maximum size of the heat rejection portion of the fin of Figure 7 for various heat rejection rates and liquid layer thicknesses, as a function of the wicking material parameter ℓ_m/K_1. Again it must be remembered that neither gravity nor the evaporator section size are considered.

Some idea of the relative magnitudes of ℓ_m and K_1 can be obtained from the tabulated values listed in Table 1. The inequality signs in the table refer to tests in which the sample size was too short to allow water to rise to the equilibrium height ℓ_m. It can be seen that a good wicking material can have a value of ℓ_m/K_1 at least as high as .93 $\times 10^{-9}$ ft^3. These tabulated values of ℓ_m/K_1 can be used in conjunction with Figure 10 to obtain an idea of maximum fin sizes.

TABLE 1

Wicking Parameters for Water (70°F)

Sample	ℓ_m, feet	K_1 1/ft^2	ℓ_m/K_1 ft^3	
cellulose sponge	0.386	$7.16 \times 10^{+9}$	0.0539×10^{-9}	conventional wicking materials (Ref. 7)
silica vitreous fiber (batt)	0.812	$9.40 \times 10^{+9}$	0.0865×10^{-9}	
Orlon	0.708	$7.51 \times 10^{+9}$	0.0941×10^{-9}	
viscous rayon	>0.666	$1.67 \times 10^{+9}$	$>0.40 \times 10^{-9}$	
silica vitreous fiber (bulk)	>1.00	$1.08 \times 10^{+9}$	$>0.926 \times 10^{-9}$	
nickel fibrous metal 24% dense	>0.834	$11.48 \times 10^{+9}$	$>0.0733 \times 10^{-9}$	metallic wicking materials (P&WA preliminary data)
powdered sintered metal (nickel) (20 μ filter rating)	>0.791	$13.22 \times 10^{+9}$	$>0.0598 \times 10^{-9}$	

TABLE 1 (Cont'd)

Sample	ℓ_m, feet	K_1 $1/ft^2$	ℓ_m/K_1 ft^3	
powdered sintered metal (nickel) (100 μ filter rating)	>0.458	$1.93 \times 10^{+9}$	$>0.238 \times 10^{-9}$	metallic wicking material (P&WA preliminary data)

The simplified analytic model of the vapor-chamber fin presented in this section illustrates the need for a separate wicking study to determine the value of ℓ_m/K_1 for various wicking materials. Such a study is now being conducted and will be explained in the next section.

E. Summary

In the present study of the vapor-chamber fin for use in space-radiator applications, the two key factors in the operation of the fin as a heat rejection device seem to be:

1) The heat flux at which apparent film-boiling occurs in the wick of the evaporator section of the fin, and

2) The maximum liquid flow rate that the capillary pump can provide to the evaporator section of the fin.

Due to the complicated nature of the phenomenon of boiling itself, a separate experimental program is being conducted to evaluate the limits imposed on fin operation by the onset of boiling in wicks.

To evaluate the effect of the capillary pump on fin operation, a simplified analytic model has been derived in which it was found that the output of the capillary pump depends on the liquid parameter

$$N = \frac{\rho_L \, h_{VL} \, \sigma}{\mu_L} \tag{47}$$

and the wicking material parameter

$$\frac{\ell_m}{K_1}$$

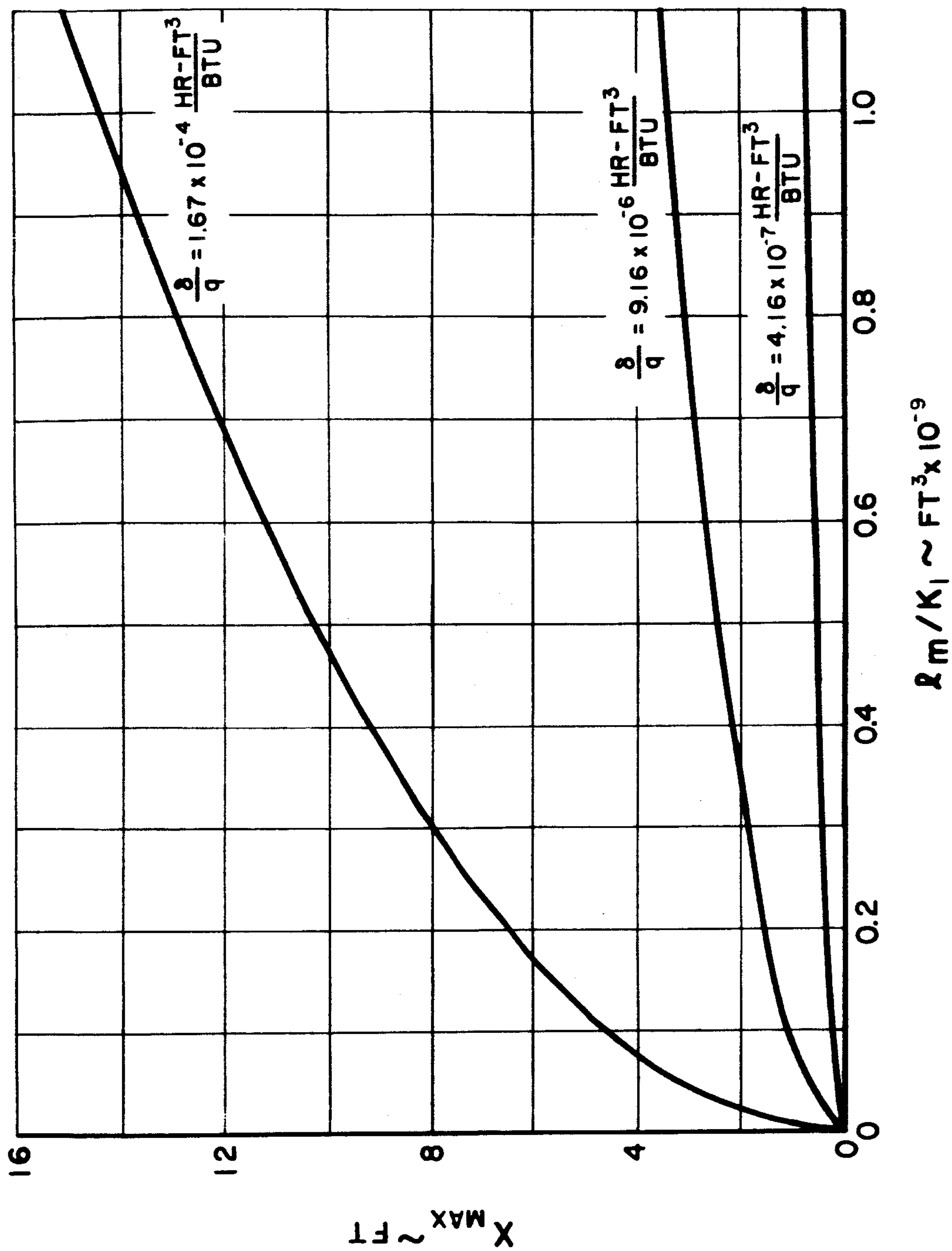

Figure 10 Maximum Fin Length vs Wicking Parameter for Water at 70°F

Both of these parameters should be large to maximize the performance of the vapor-chamber fin.

The wicking material parameter is the ratio of the maximum capillary forces to the frictional forces on a liquid flowing in a wick. The constant ℓ_m is a measure of the magnitude of the capillary forces associated with the liquid-wick combination. Physically, ℓ_m is the equilibrium height to which the liquid will rise in a vertical sample of the wick.

The constant K_1 is a measure of the magnitude of the frictional forces associated with a flow of the liquid through the wick. This constant is obtained by measuring the pressure drop across a wicking material sample through which a given amount of liquid is flowing.

Thus to study the effect of the capillary pump on the operation of the fin, a separate wicking materials study is being conducted to measure values of ℓ_m and K_1.

IV. VAPOR-CHAMBER FIN WICKING MATERIALS AND LIQUIDS

A. Wicking Materials

Before discussing the wicking materials that are being studied, some terms concerning porous media will be defined.

The porosity of a material, ϵ, is the total void volume of a sample divided by the total volume of the sample. Thus a porosity of 0 per cent denotes a solid substance containing no voids (pores) and one of 100 per cent denotes a complete void. While the porosity accounts for all voids or pores in a sample, the effective porosity is based upon the connected (as opposed to separate or unconnected) pore space within the sample. Because of the nature of the porous media that will be dealt with in this study, it will be hereafter assumed that the porosity is equal to the effective porosity.

The free flow area ratio F_{AR} is defined as the ratio of area available to flow of a fluid at any given cross-section of the porous material, divided by the total cross-sectional area. The free-flow area ratio could be obtained by photographing the cross-section of a porous material and measuring the pore area over a given total area. However for a material that is isotropic and for which the effective porosity is equal to the porosity, a value of F_{AR} can be defined by considering a unit cube of the porous material and assuming that the mass of this porous cube can be compressed into a smaller solid cube. The free-flow area ratio can then be computed, based on the frontal area of the porous cube and the solid cube. This results in

$$F_{AR} = 1 - (1 - \epsilon)^{2/3} \qquad (48)$$

Hereafter, when dealing with isotropic materials, this equation will be used to calculate F_{AR}.

The pore size distribution function $\alpha(r)$ can be defined by the equation

$$dV = \alpha(r) \ dr \qquad (49)$$

where dV is the volume of the pores of radii between r and r + dr. A typical plot of $\alpha(r)$ is shown in Figure 11, together with the mean pore radius. Once a good wick is found it will be of great interest to see exactly what type of pore size distribution curve it has, that is, whether the curve is broad, narrow, flat, etc.

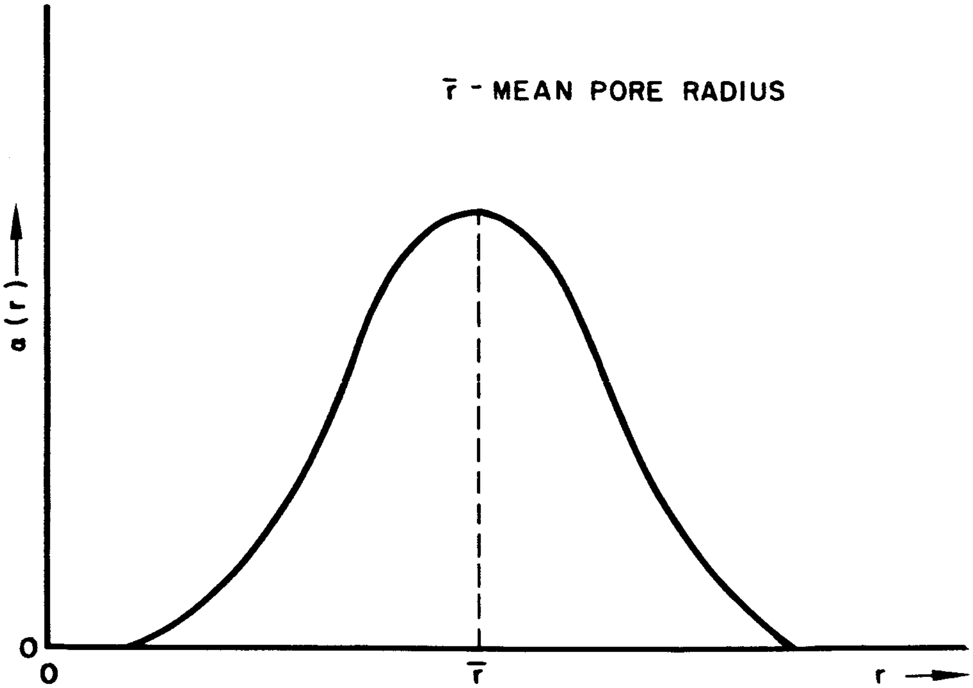

Figure 11 Pore Size Distribution Curve

An equivalent diameter D_c can be defined in such a way as to characterize the frictional properties of a wicking material sample. For a given flow rate of liquid through the wicking material, the resulting pressure drop ΔP over a given sample length Δx can be expressed in terms of the Poiseuille equation for flow in a tube, to get

$$\frac{\Delta P}{\Delta x} = \frac{32 \, \mu_L \, u_\epsilon}{D_c^2} \tag{50}$$

where μ_L is the liquid viscosity, u_ϵ is the average liquid flow velocity through the pores of the material and D_c is the equivalent diameter. As defined here, D_c is a variable that contains the effects of tortuosity, interconnectiveness of the pores, and an average pore shape factor and size.

The above expression can be combined with Equation (24) to obtain

$$D_c = \left(\frac{32}{F_{AR} K_1} \right)^{1/2} \tag{51}$$

where K_1 is the wick friction factor, defined by Equation (24). The methods of obtaining K_1 are discussed in Sections V. A. to V. D. The flow velocity does not appear in the above expression for D_c because of the relation between u_L, the bulk liquid velocity, and u_ϵ, given by

$$\frac{u_L}{u_\epsilon} = F_{AR} \tag{52}$$

where F_{AR} is the free-flow area ratio.

The equivalent diameter D_c can be compared with the pore size distribution curve values for a porous material, to obtain some idea of the effects of tortuosity, pore interconnectivity, and average pore shape factor and size on the flow through a wicking material sample. For instance if tortuosity is high, D_c will be much smaller than the value of the mean pore size given by the distribution curve. D_c will also provide a convenient characteristic dimension on which to base a Reynolds number describing the flow through a sample.

The following list of porous materials is being evaluated in the wicking studies (described in Section V), and the boiling studies (described in Section VI). Out of this list at least two porous materials will be selected for use in experimental vapor-chamber fin models.

1) Sintered and Nonsintered Layers of Metallic Screens

Composed of a sandwich of several layers of screens which have either been sintered or welded together.

porosity - 75 to 36 per cent depending on wire diameter and type of stacking

free-flow area - 12 to 32 per cent depending on wire diameter, type of stacking, and flow direction

2) Sintered Random Fibrous Metallic Structures

A randomly interlocked structure of metallic fibers that have been sintered together at their points of contact. A sample can be made denser by rolling.

porosity - 95 to 0 per cent depending on fiber diameter and packing

free-flow area - 0 to 86 per cent depending on fiber diameter and packing

3) Sintered Powdered Metals

Composed of spherical or near-spherical particles that have been sintered together at their points of contact. A sample can be made denser by rolling.

porosity - 60 to 0 per cent depending on packing

free-flow area - 0 to 46 per cent depending on packing

4) Flame-Sprayed Powdered Metals

Composed of a powdered metal-salt mixture that is flamed-sprayed onto a solid surface. The salt is leached out, leaving a porous metallic structure.

porosity - 50 to 0 per cent depending on amount of salt used

free-flow area - 0 to 37 per cent depending on amount of salt used

The metals used in the above list are nickel as a first choice, and stainless steel if the latter is not available. Both oxidized and unoxidized samples will be tested.

The porous materials listed were chosen on the basis of the following properties:

1) Wetting Properties

For a porous material to act as a wick, it must be wetted by the liquid. With average care in eliminating contaminents, nickel forms a zero contact angle (i. e, completely wetting) with the conventional liquids used in this study. Nickel oxide is even more likely to form a zero contact angle than pure nickel, because of its higher surface energy.

Because stainless steel is also completely wetted by most liquids, it will be employed as a second choice. However much greater care must be taken with a stainless steel surface to insure that no contaminants are present to prevent wetting. The need to keep stainless steel expecially clean has been pointed out by Fox, Hare, and Zisman [12].

2) Chemical Activity

Nickel, stainless steel, and their oxides are inert with respect to the working fluids of this study.

3) Fin Fabrication

Any sample tested may eventually be installed in a fin model. All of the porous materials listed are capable of being attached to the metal surface of the fin cavity and are capable of being fabricated in a variety of shapes. Metallic wicks were therefore selected since meeting both of these requirements with a ceramic wicking material would be more difficult.

4) Dimensional Stability

As shown by the analytic model of the last section, the wick dimensions must be known with some accuracy. All of the above materials are sufficiently rigid so that they will maintain their dimensions when saturated with a liquid. This is not true of soft fibrous and woven materials such as Fiberglas, textile fabrics, etc. The latter materials may either swell upon absorbing liquid or become compressed by capillary forces at a liquid-solid-vapor interface.

Sample rigidity also allows the pore size distribution to be determined, since there are no experimental techniques for measuring this quantity in nonrigid porous materials.

5) Isotropy

As pointed out in Section III.C. it is essential that an isotropic wicking material be used. By isotropic, it is meant that the wicking material has the same pore size distribution in any given direction. Thus, by using isotropic wicks, the operation of the capillary pump can be studies without complications caused by wick directional properties.

The porous materials listed are essentially isotropic, with the obvious exception of the metallic screen layers. An analysis of the latter shows that for a square weave structure, the departure from isotropy is not great.

6) Wick Thermal Conductivity

A factor in fin performance that has not been discussed yet is the importance of the thermal conductivity in the liquid-wick layer. The effective thermal resistance of this layer is reduced if a wicking material of relatively high thermal conductivity is used.

This is shown by considering the two limiting cases of heat conduction in a porous medium. The lower limit on the effective conductivity of a two-phase porous medium is found by assuming that the two phases conduct heat in series. The resulting expression is

$$\left(\frac{k}{k_s}\right)_{min} = \frac{1}{1 + \epsilon\left(\frac{k_s}{k_L} + 1\right)} \tag{53}$$

where k is the effective thermal conductivity, ϵ is the porosity, and k_s and k_L are solid and liquid conductivities respectively. To maximinize k, k_s should be as large as possible.

The upper limit on the effective heat conductivity would occur if both phases conducted heat in parallel. This yields

$$\left(\frac{k}{k_s}\right)_{max} = 1 - \epsilon\left(1 - \frac{k_L}{k_s}\right) \tag{54}$$

Again, k_s should be as large as possible to maximize k, the effective conductivity.

Hence, from the standpoint of wick thermal conductivity, metal porous materials will be superior to other more conventional wicking materials, due to their inherently higher conductivities.

B. Test Fluids

As shown by Equation (42), the liquid properties enter into the operation of the vapor-chamber fin as the dimensional parameter N, defined as

$$N \equiv \frac{\rho_L \, h_{VL} \, \sigma}{\mu_L}$$

where ρ_L is the liquid density, h_{VL} is the latent heat of vaporization, σ is the liquid-vapor surface tension, and μ_L is the liquid viscosity.

To maximize the heat transport properties of the fin, N should be as large as possible. Also, the test liquid should have a significant vapor pressure in the temperature range 200 - 500°F. Otherwise any experimental fin model using such a fluid will operate at too low a heat input, causing the experimental uncertainties to be too high. Similarly, the liquid vapor pressure in this temperature range should not be too high, or the fin models will become pressure vessels with prohibitively thick walls.

Values of N for a number of liquids that meet these requirements are listed in Table 2.

TABLE 2

Properties of Various Liquids

Fluid	Vapor Pressure At 300°F, psia	Boiling Point At 1 atm, °F	N, $\frac{\text{Btu hr lb}}{\text{ft}^3\ \text{lb}_m}$
water	67.0	212	124.4
trichloroethylene	77.4	188.4	13.4
ethyl alcohol	143.0	170.5	9.49
perchloroethylene	31.9	250.2	9.33
Dowtherm E	6.5	352.0	6.26
Freon 113	180	117.6	5.30
Freon 114B2	185	117.1	5.03
Freon 112	67.0	199.0	4.81
Dowtherm A	0.638	495.8	2.02
FC-75	50.0	214.0	1.55
ethylene glycol	2.71	387.5	1.06
diethylene glycol	0.503	474	0.707
FC-43	9.0	337	0.281

The values listed in this table show water to have one of the highest values of N for conventional liquids, in addition to having a favorable vapor pressure - temperature relationship. Hence water will be the primary test fluid.

To evaluate the effect of the variation of N on the heat transfer properties of the fin, one other liquid will be tested. The second fluid must satisfy the conditions given above and have a value of N significantly lower than that of water, although not low enough to drastically reduce the heat input to the fin, see Equation (43), and thereby cause the experimental uncertainties to become too high. Also the fluid should have a fairly complete tabulation of properties and be compatible with the wicking material. Because it will be tested in the atmosphere during the wicking and boiling tests it must be relatively nonreactive and nontoxic.

Of the liquids listed in Table 2, Freon 113 seems to best satisfy these requirements and thus will be used as the second fluid to evaluate the effect of N on the operation of the vapor-chamber fin.

V. WICKING STUDIES - TASK 1

A. Permeability of Wicks

A wicking material will act as a liquid pump because of the capillary forces produced by the interaction of the liquid and the matrix material of the wick. However, an evaluation of a given wicking material as a capillary pump is incomplete without knowledge of the drag forces necessarily associated with any flow through the wick. Thus a wicking material can be evaluated as a capillary pump by its net output, where

$$\text{capillary pump output} \propto \frac{\text{capillary forces}}{\text{frictional forces}} \tag{55}$$

As shown in Section III, D., this ratio can be expressed as

$$\text{capillary pump output} \quad \propto \quad \frac{\ell_m}{K_l} \tag{56}$$

In this equation ℓ_m is the equilibrium height obtained from the wicking test described in Section V. F., and K_l, the wick friction factor, is defined by Equation (24).

The object of the permeability tests is to determine the wick friction factor K_l for various wicking materials. As defined in Equation (24), K_l is the reciprocal of permeability, or

$$K_l = \frac{1}{\text{permeability}} \tag{57}$$

with the units of $(\text{length})^{-2}$.

As shown by Equation (24), K_l can be measured by putting a known flow rate through a rectangular wicking sample of known size. The pressure drop across the sample can be measured, and K_l can then be calculated from the expression

$$K_l = \left(\frac{A_c}{\Delta x}\right)\left(\frac{\rho_L}{\mu_L}\right)\left(\frac{\Delta P}{w_L}\right) \tag{58}$$

where A_c is the total flow cross-sectional area of the sample, Δx is the length of the sample, ρ_L and μ_L are the liquid density and viscosity, ΔP is the pressure drop across the sample, and w_L is the liquid flow rate.

As mentioned in Section III. D., K_l is dependent on the geometry and dimensions of the passages in the wicking material.

In the range of low liquid flow rates encountered in the vapor-chamber fin, Darcy's law[6] for flow through porous media will apply, meaning that K_l should be independent of the flow rate.

The upper limit on the flow rate for permeability testing can be determined from an estimate of the maximum flow rate that could occur in a vapor-chamber fin. This maximum liquid flow rate can be calculated by assuming that the minimum radius of curvature of the liquid-vapor interface occurs in the matrix of the wick. Shown in Figure 12 is a rectangular piece of wicking material acting as a capillary pump.

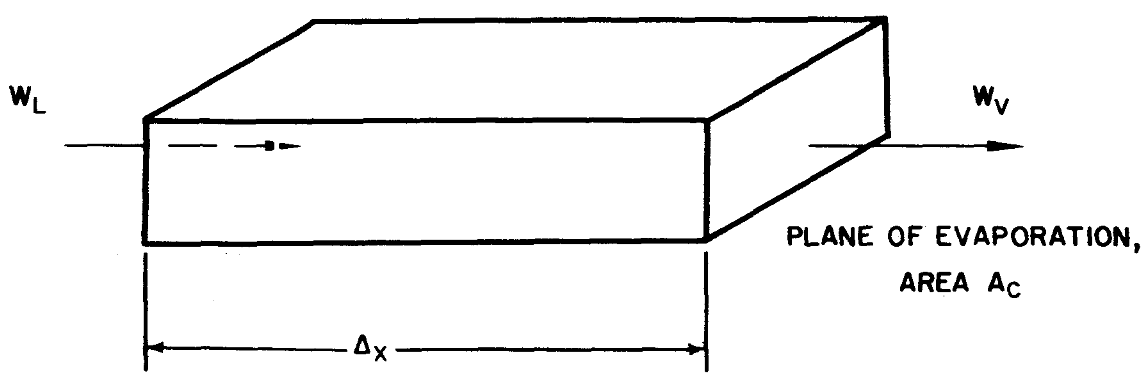

Figure 12 Model of a Capillary Pump

At the front face, liquid is being evaporated at such a rate that the wicking material is providing a maximum flow. If this is true, then the pressure drop across the liquid-vapor interface at the plane of evaporation is

$$(\Delta P) = \frac{2\sigma}{R_{min}} \qquad (59)$$

where R_{min} is the minimum radius of curvature that the wick can support and σ is the surface tension. By using Equation (44) this becomes

$$(\Delta P)_\sigma = \frac{g}{g_o} \rho_L \ell_m \qquad (60)$$

where ℓ_m is the maximum length that a liquid will wick up to in a vertical sample of the porous material. This pressure drop must be balanced by the frictional pressure drop caused by the flow of liquid through the wick, so that

$$(\Delta P)_\sigma = (\Delta P)_f \tag{61}$$

Combining Equations (59) and (58) yields an expression for the maximum flow rate in the wick structure of Figure 12, of

$$(w_L)_{max} = \frac{g}{g_o} \frac{\rho_L^2}{\mu_L} \frac{A_c}{\Delta x} \frac{\ell_m}{K_1} \tag{62}$$

where
- g = acceleration of gravity
- g_o = Newton's second law proportionality constant
- ρ_L = liquid density
- x = flow length
- A_c = total cross-sectional flow area

Thus in any test to evaluate K_1 in a range that is applicable for the vapor-chamber fin, the flow rate should not exceed the value given by Equation (62), where ℓ_m has been measured for the material that is being tested.

The permeability investigations of Ginwala, Blatt, and Bilger[7] show that in their work K_1 is initially constant with time, but increases in magnitude after a certain amount of flow has passed through the wicking material. This phenomenon seems best explained by assuming that tiny gas bubbles are presented in the liquid in the wick. If these bubbles stick in the matrix of the wicking material, they might decrease the effective flow area in the wick and increase K_1. The same thing could have been true if foreign particles were present in the liquid. The permeability apparatus described in the next section has been designed to eliminate these problems.

B. Description of the Permeability Apparatus

A schematic diagram of the permeability apparatus is shown in Figure 13. It was designed to provide accurate low flow rates of liquid through a wicking material sample, and to minimize the effects of dissolved gases, foreign matter in the liquid, and corrosion of materials. The equipment shown in Figure 13 includes tubing, valves, filter, accumulator tank, pump, flowmeters, heaters, coolers, and a wick specimen holder. Liquids used are listed in Section IV. B.

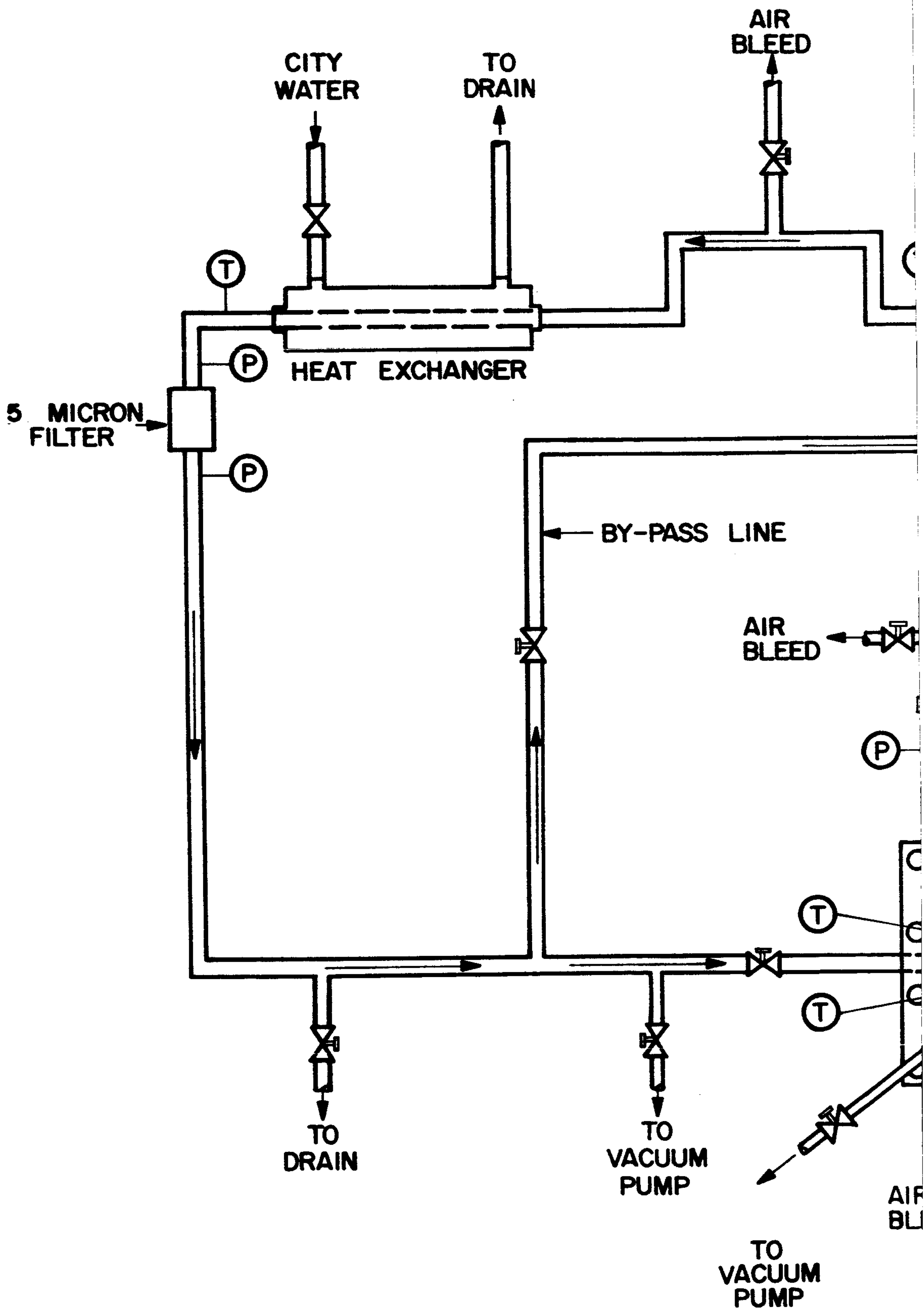

Figure 13 Schematic Diagram of Permeability Apparatus

#1

-2698

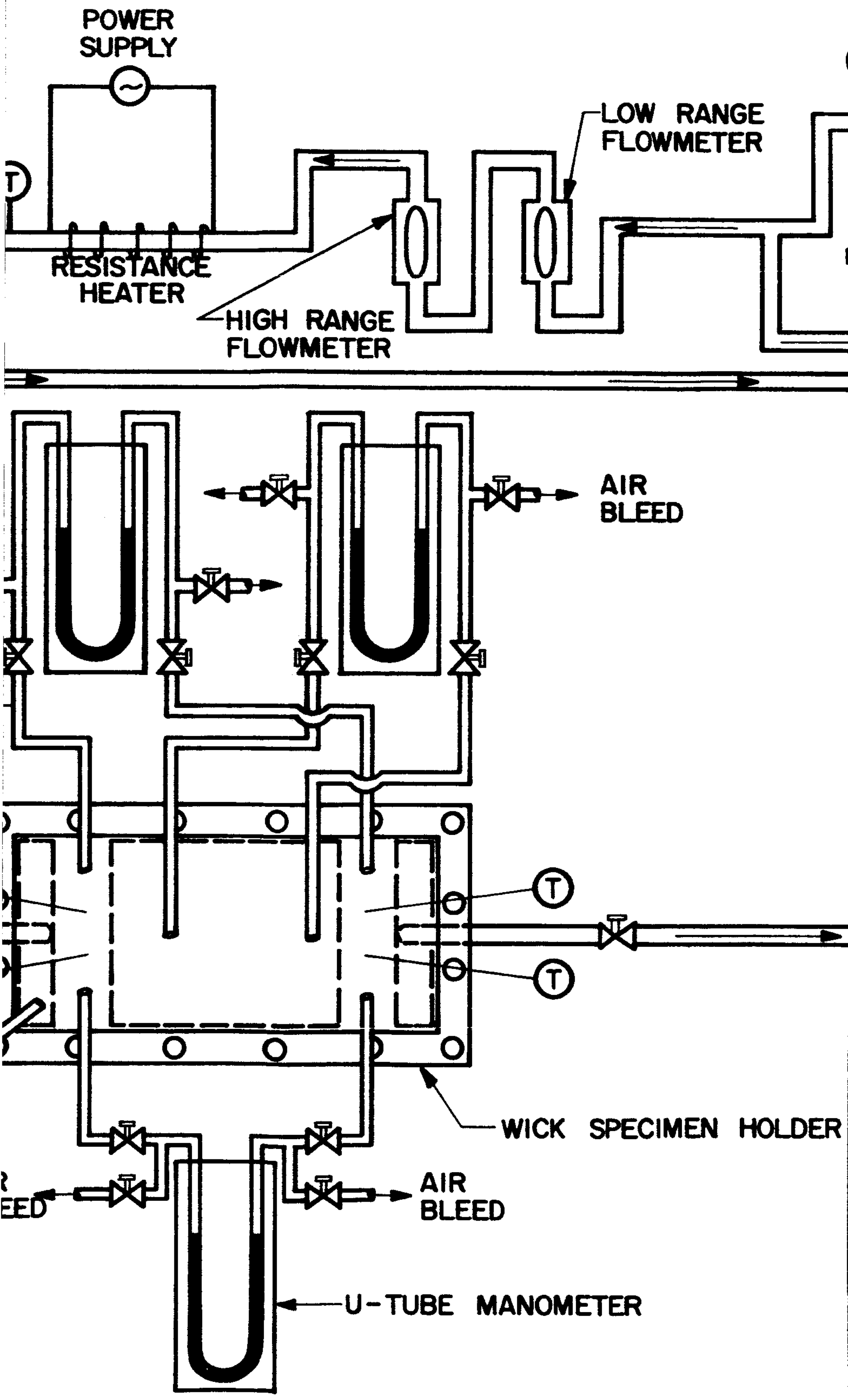

POWER
SUPPLY
LOW RANGE
FLOWMETER
RESISTANCE
HEATER
HIGH RANGE
FLOWMETER
AIR
BLEED
WICK SPECIMEN HOLDER
AIR
BLEED
U-TUBE MANOMETER

2

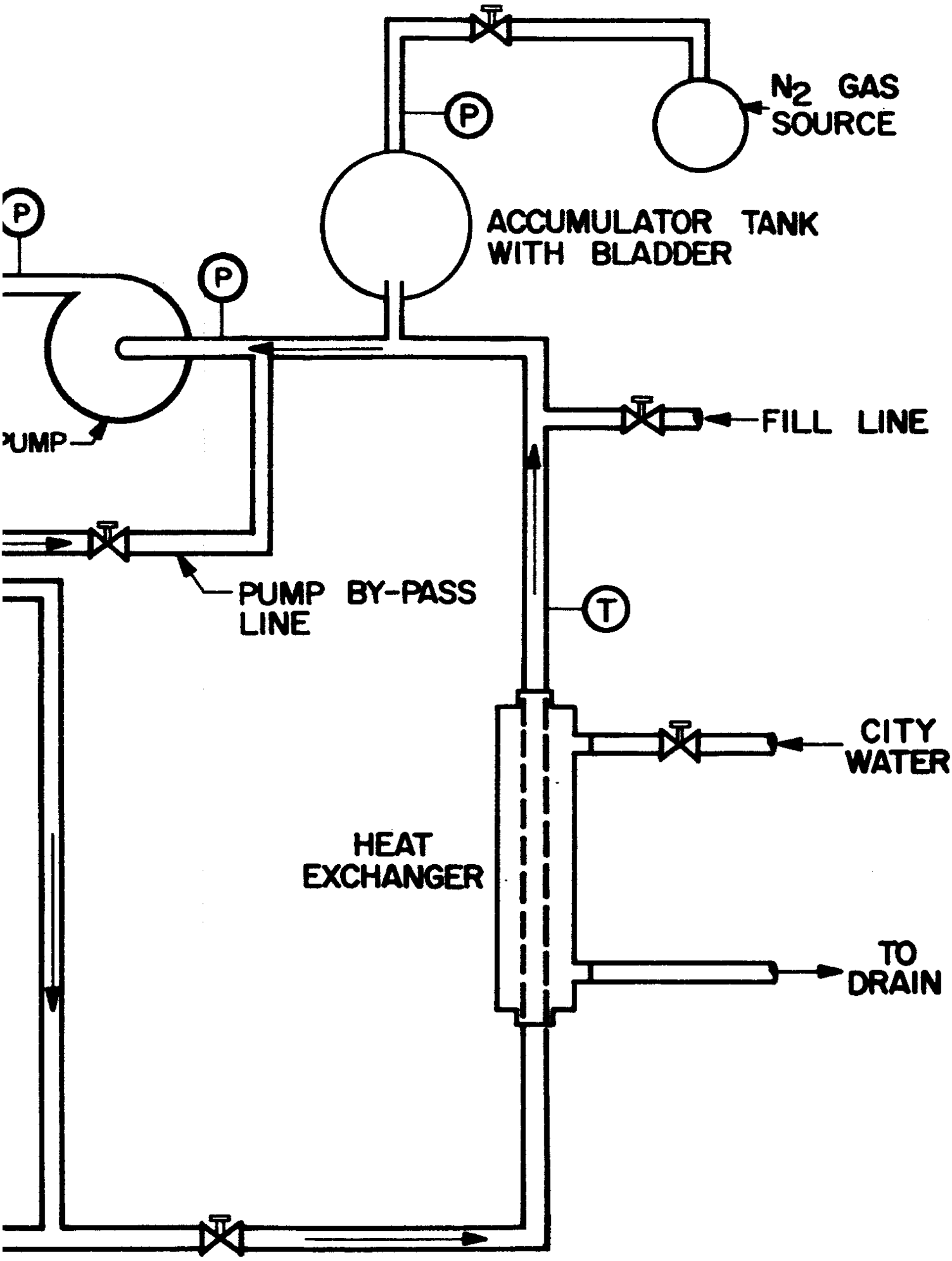

N_2 GAS SOURCE
P
ACCUMULATOR TANK WITH BLADDER
P
P
FILL LINE
PUMP
PUMP BY-PASS LINE
T
CITY WATER
HEAT EXCHANGER
TO DRAIN
FLOW CONTROL VALVE

The tubing is one-quarter inch, 316 stainless steel tubing, chosen for its corrosion-resistant properties. The valves used throughout the system are made of 316 stainless steel also. The filter is made of 316 stainless steel sintered powder metal and has a five-micron filter rating. The filter will prevent microscopic foreign material from lodging in the wick test sample. The heaters and coolers used are constructed of stainless steel material to prevent corrosion in the system.

The accumulator tank is a standard 2 1/2-gallon high pressure hydro-pneumatic transfer barrier accumulator. During operation, the working fluid will be only in contact with the Buta-N bladder or the stainless steel inserts and fittings associated with the bladder. Any desired pressure level in the system can be set, and yet a separation can be maintained between the pressurant gas and the working fluid. This separation of the gas and liquid prevents the gas from dissolving in the liquid, thus maintaining a gas-free system.

The pump for the system is a sealless positive-displacement gear pump. This type of pump prevents leakage of air into the system and working fluid leakage from the system. The impeller gears are made of Teflon and the housing material is stainless steel. The drive coupling between motor and pump is magnetic through a solid wall.

The flowmeters are Fisher-Porter Tri-Flat variable-area flowmeters. Two flowmeters will be used to insure proper accuracy for high and low flow. The approximate range of the low range meter is 0.02 to 1.4 pph of water, while the approximate range of the high range meter is 0.2 to 15 pph of water.

The wick sample holder as shown in Figures 14, 15, and 16 was constructed of 316 stainless steel material. The holder contains the necessary fittings for measuring the temperature of the working fluid and the pressure drop of the fluid through the wick. The system was designed to allow for wick holder removal while preventing the leakage of air into the system. Upon installation of the wick holder, the holder assembly can be evacuated to minimize the transfer of entrapped air in the holder to the working fluid. Gasket material of neoprene or silicon rubber will be used to prevent leakage of the fluid around the wick sample.

Typically, the sample of wicking material will be 2 inches wide and 3 inches long in the flow direction. The porous material which will be bonded to a stainless steel backup plate will be 0.1 inch in height.

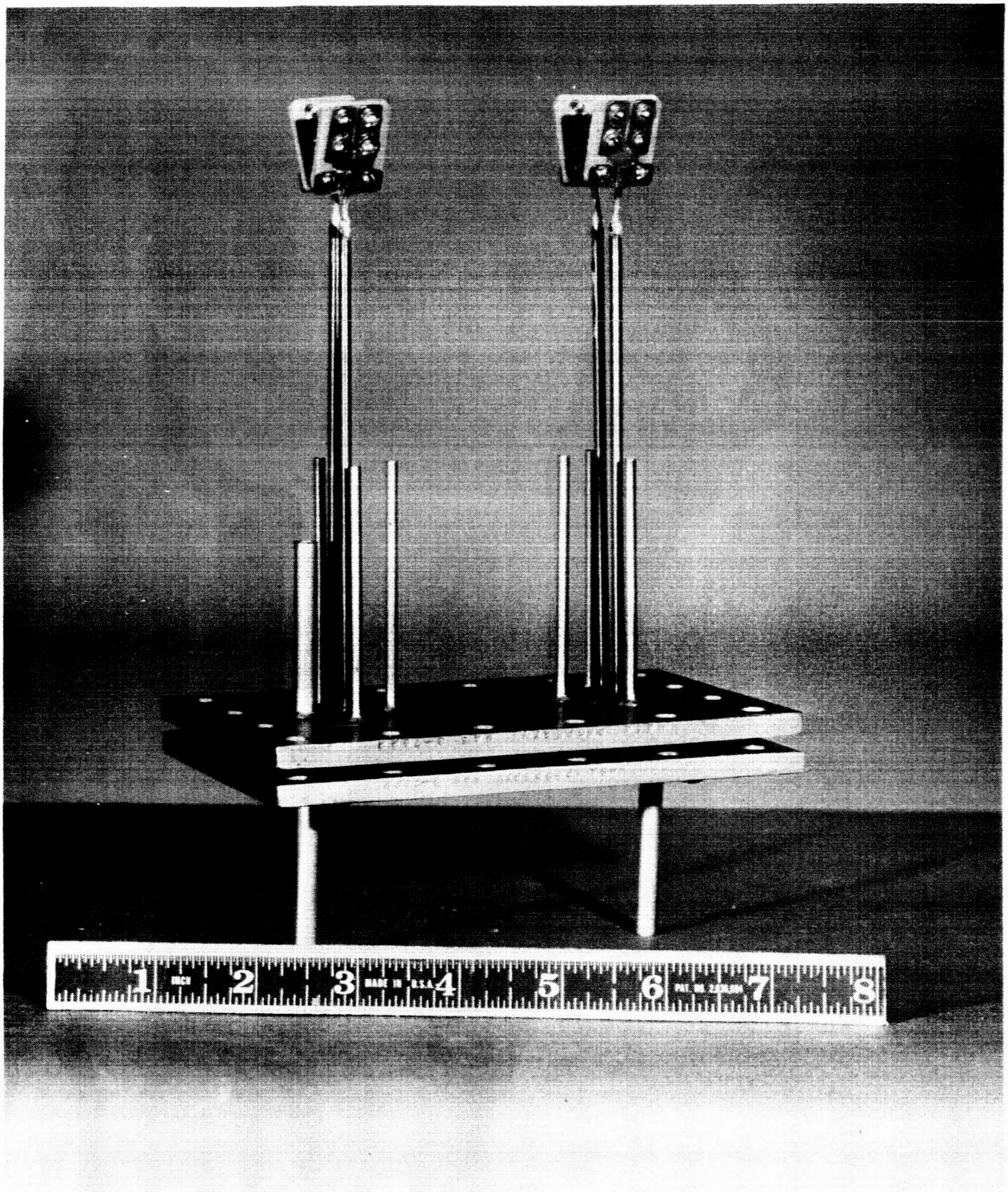

Figure 14 Assembly View of Wick Sample Holder (Gaskets not Shown)

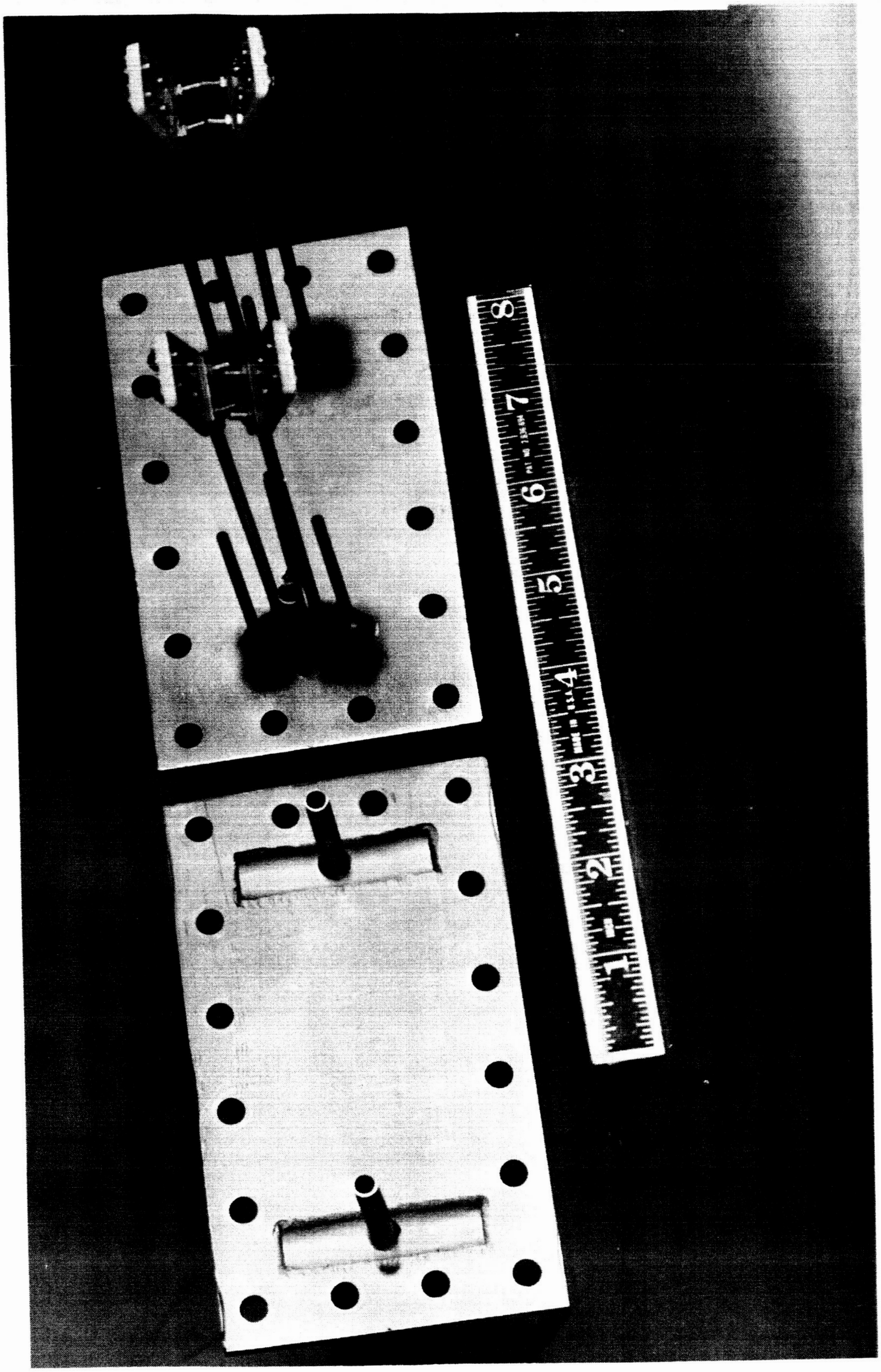

Figure 15 Outside View of Disassembled Wick Sample Holder, Showing Flow Inlet and Outlet and Instrumentation

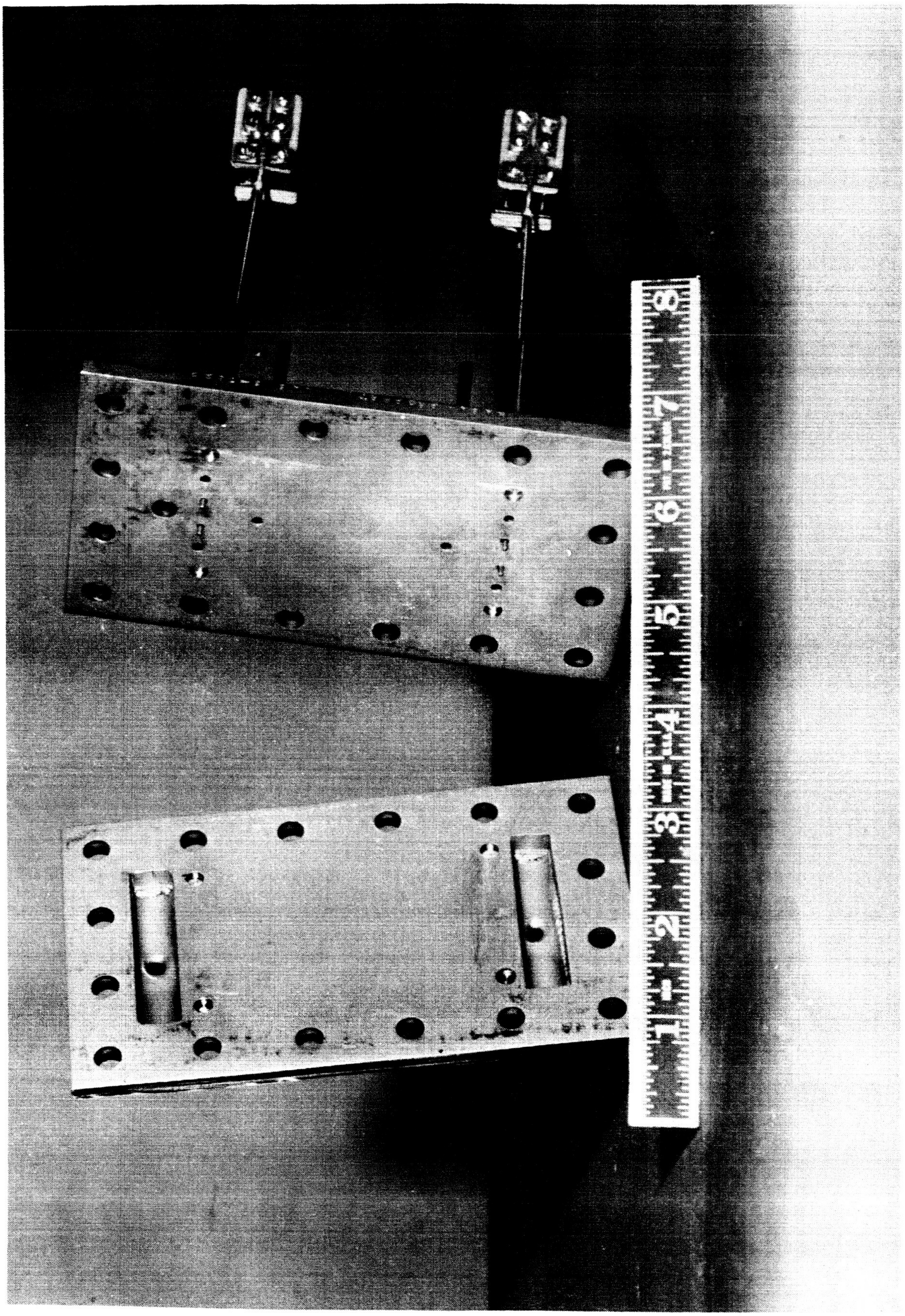

Figure 16 Inside View of Disassembled Wick Sample Holder, Showing Flow Inlet and Outlet Passages (Gaskets not Shown)

To insure that permeability data is obtained in the range of flows anticipated for fin operation, the flow rate through the wicking sample will be varied from zero to the maximum value given by Equation (62).

If for a liquid at a given temperature it is found that K_1 computed from Equation (58) is constant over this flow rate range, the liquid flow through the wick is within the regime where Darcy's equation applies.

To make certain that there is no dependency of K_1 on the liquid properties, the liquid temperature will be varied during tests on the permeability apparatus. Also, a second fluid, Freon 113, will be used with some samples that were evaluated with water.

C. Permeability Test Procedure

The major problem which must be overcome in the operation of the permeability apparatus is that of degassing the working fluid. Preventative action will be taken during fill operation and running operation to delete as much as possible of dissolved gas in the working fluid.

The fill operation will consist of evacuating the system by means of a vacuum pump to approximately 10^{-5} mm Hg. The system will then be checked for leaks. The working fluid, either water or Freon 113, will then be transferred to the system. Before transfer, the fluid will have been degassed by passing it through several boiling and condensing cycles. The fluid will be maintained at a temperature near its boiling point to maintain low gas solubility before transfer to the system.

After filling the system with the working fluid, further degassing can be done by heating the fluid near its boiling point by means of the electrical heater as shown in Figure 13. By heating, the gas solubility of the fluid will be reduced. Any excess gas released by heating can be removed from the system by venting the gas at a bleed downstream from the electrical heater. A bypass line around the wick holder can be used for the degassing operation without forcing the fluid through the wick holder.

D. Instrumentation Accuracy

The two most important measurements will be flow and pressure drop. Other less critical measurements in the system will include temperature and pressure.

The manometers chosen for measuring the pressure drop through the wick sample will be of the thirty-inch U-tube variety. Readings to the nearest 0.1 inch and estimates to the nearest 0.05 inch of fluid can be made. These manometers will contain air bleeds in each leg for removal of gas as shown in Figure 13. Special manometer taps (see Figure15) have been located on the wick holder to obtain a pressure drop measurement within the wick, thus removing any entrance or exit effects. The pressure drop is expected to range between 0 and 20 inches of manometer fluid. Two other manometers will measure the pressure drop through the entire wick sample. The fluid to be used in the manometers will be acetylene tetrabromide, chosen for its specific gravity (2.9381 at 80°F) and its immiscibility with water.

The flowmeters chosen for flow measurement are Fisher-Porter Tri-Flat variable-area meters. Two meters were selected to cover the low and high-flow ranges, which are 0 to 1.45 lb_m/hr and 0 to 14 lb_m/hr respectively. A variable scale on the tubes of the meters prevents calculation of a single exact accuracy of reading over the entire scale. Thus, the low-range flowmeter is accurate to ± 7 per cent at a flow of 0.4 lb_m/hr and ±1.8 per cent at 1.45 lb_m/hr, while the high-range flowmeter is accurate to ±5 per cent at 1.45 lb_m/hr and ±1 per cent at 14 lb_m/hr.

Temperature measurements will be made using chromel-alumel thermocouples connected to a Honeywell Brown Electronik readout instrument. The accuracy of this system is estimated to be ±2°F. Pressure measurements will be made using Bourdon-tube type gages with a maximum scale reading of 30 psig. Scales are in 0.2 psi increments and readings can be estimated to the nearest 0.1 psi. These gages have bleed ports for removal of entrapped gases in the lines. Experimental pressures will be in the range of 3 to 15 psig.

The experimental uncertainties in flow rate and pressure drop combine to give an expected uncertainty in K_1 of about ±2 to ±7 per cent.

E. Permeability Apparatus Construction Progress

To date, all parts for the construction of the apparatus have been received. Preliminary construction of the housing for the various components of the system is almost complete. No immediate delays or problems with construction of the apparatus are expected.

F. Wicking Rise Tests

The purpose of the wicking rise tests is to determine the maximum height to which a liquid will rise in a given vertical wicking material sample and thereby obtain a measure of the minimum liquid-vapor interfacial radius of curvature that the material will support. As shown in the derivation of the fin model in Section III. D., the value of this curvature, R_{min}, is needed to evaluate the maximum pumping force produced by the wicking material. This maximum pumping force, expressed as a differential pressure is

$$(\Delta P)_\sigma = \frac{2\sigma}{R_{min}} \tag{63}$$

Thus by evaluating R_{min} for a given wicking material, the maximum pumping force of the wick is evaluated. The frictional forces associated with the liquid flow caused by the pumping force are evaluated in the permeability tests described in Sections V. A. through V. E.

The wicking rise test is a simple method of determining the effective minimum radius of curvature that a wicking material can support. As an explanation, the wick and liquid reservoir shown in Figure 17 can be considered.

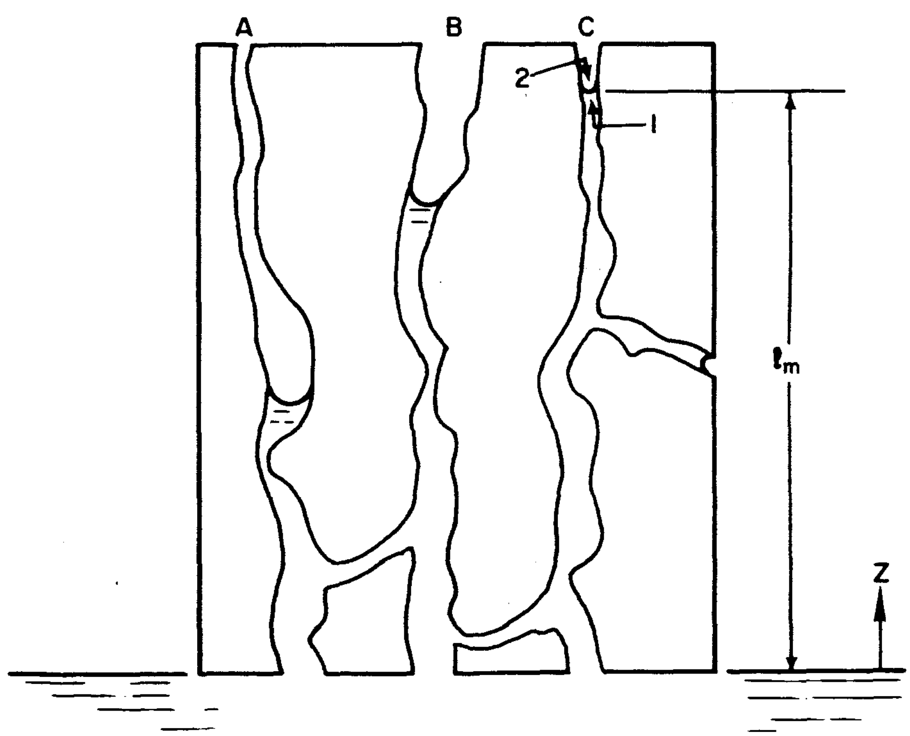

Figure 17 Equilibrium Condition for Three Selected Pores in Saturated Wick

In the porous material shown in Figure 17, only three connected pores are pictured out of the many that actually contain liquid. It is assumed that the material of this wick is one of those listed in Section IV. A. Thus, due to the properties of isotropy and homogeneity, at any given height z in the wick, all pore sizes from the smallest to the largest will be represented.

In Figure 17 the liquid has risen to an equilibrium height in each of the pores and it is observed that the liquid front in the wick has risen in some pores to a maximum height ℓ_m represented by pore C. It should be noted that in a wicking rise test, the degree of wick saturation decreases with increasing z, because fewer and fewer pores have small enough radii at a given z to provide the capillary forces necessary to overcome the increasing effects of the fluid weight.

By employing the laws of hydrostatics in the equilibrium situation pictured, the pressure in the liquid of pore C at point 1 just under the meniscus is

$$P_1 = P_a - \frac{\rho_L g}{g_c} \ell_m \tag{64}$$

where P_a is the pressure on the liquid reservoir at z = 0. Equation (64) holds no matter what the shape and size of pore C is, or how many connections it has with other pores and the free surface of the wick.

If the very small vapor head between z = 0 and point 2 just above the meniscus is neglected, then

$$P_2 = P_a \tag{65}$$

The pressure difference across the meniscus in pore C is then

$$P_2 - P_1 = \frac{\rho_L g}{g_c} \ell_m \tag{66}$$

But the Laplace-Young Equation (see Section III. D.) gives the pressure difference across the meniscus as

$$P_2 - P_1 = \frac{2\sigma}{R_c} \tag{67}$$

where it is assumed that pore C can be characterized by one value of the radius of interfacial curvature, R_c.

By equating Equations (66) and (67) it is seen that

$$R_c = \frac{2g_c \sigma}{\rho_L \, g \, \ell_m} \tag{68}$$

Since ℓ_m is a maximum for the sample and all pore sizes are present at any given z

$$R_c = R_{min} \tag{69}$$

where R_{min} is the minimum radius of curvature that the wicking material can support. Thus the wicking tests are a means of determining R_{min}.

The above assumes of course that the liquid wets the porous material of the wick, i.e., has a contact angle $0 \leq \theta < 90°$. The wicking test is not a measure of the minimum pore size of the wicking material, because a definite value of the contact angle would have to be known to calculate this. It merely permits an evaluation of the maximum capillary forces that a given liquid-wicking material combination will produce.

Thus two different wicking materials with exactly the same pore structure could conceivably have different equilibrium heights with a given liquid, due to differences in their wetting characteristics. The wicking rise tests take into account both wetting characteristics and pore size and structure, thus yielding a measure of the maximum capillary pumping forces.

G. Description of the Wicking Rise Apparatus

A photograph of the wicking rise apparatus is shown in Figure 18. The test rig consists of up to ten stoppered glass tubes of 60 mm inside diameter which are clamped vertically to a laboratory support frame and are open at the bottom. The sample is suspended in the tube along with a scale and a thermometer. The liquid is contained in a reservoir (a glass tray) that is large enough to maintain a nearly constant level while tests are in progress.

The bottom of each tube is submerged below the surface of the liquid in the reservoir, thereby sealing the stoppered tube and wetting the lower portion of the wicking sample. The atmosphere in the tube becomes saturated, preventing any net evaporation from the wick during the time and after the liquid has risen to the equilibrium height. With some samples this time may be on the order of days.

The samples vary in length from about 6 to 24 inches depending on the individual wicking capability. Each wick sample is sintered to a nickel backup plate to simulate the actual construction in a vapor-chamber fin application.

H. Wicking Rise Test Procedure and Accuracy

A wicking rise test begins by lowering a glass tube containing the sample about 1/4 inch into the liquid. The air in the tube is compressed slightly, keeping the liquid level below the end of the sample. A run is then begun by opening a stopcock at the top of the tube, which allows the liquid reservoir level to rise up about 1/8 inch on the wick sample. Simultaneously a stopwatch is started and a rate of liquid rise curve is obtained by noting the time that it takes for the liquid front to reach specified levels.

To insure the determination of a true value of ℓ_m, test data is taken until no more increase in the level of the liquid front is noted for a considerable period of time. Some difficulty has been found in visually observing where the liquid front is in many samples. Various methods, such as using dyes and fluorescent liquids radiated with ultraviolet light were tried, but to no avail. The best method found to date is one using strips of litmus paper clipped to the wick. As the liquid front advances up the wick, the litmus changes to a darker shade of pink. There is a slight lag in the response of the litmus paper for times close to zero, but this does not affect the final accuracy of the test, since ℓ_m is an equilibrium height and not time-dependent.

The final equilibrium height ℓ_m can be read to ±1/16 inch in a possible 6 to 24 inches.

I. Results and Progress of the Preliminary Wicking Rise Tests

Thus far the wicking rise tests have been used to evaluate classes of wicking materials. This has been done by obtaining samples from a large number of vendors. By running a wicking rise test on each of those samples and obtaining a rate of rise curve for each, a rough idea can be obtained of their relative wicking ability. On the basis of these preliminary wicking tests, more elaborate samples have been ordered that can be used in the wicking rise tests, the permeability tests and the wick boiling tests. Such a procedure was necessary because of the relative expense of each of the classes of metallic porous materials listed in Section IV. A.

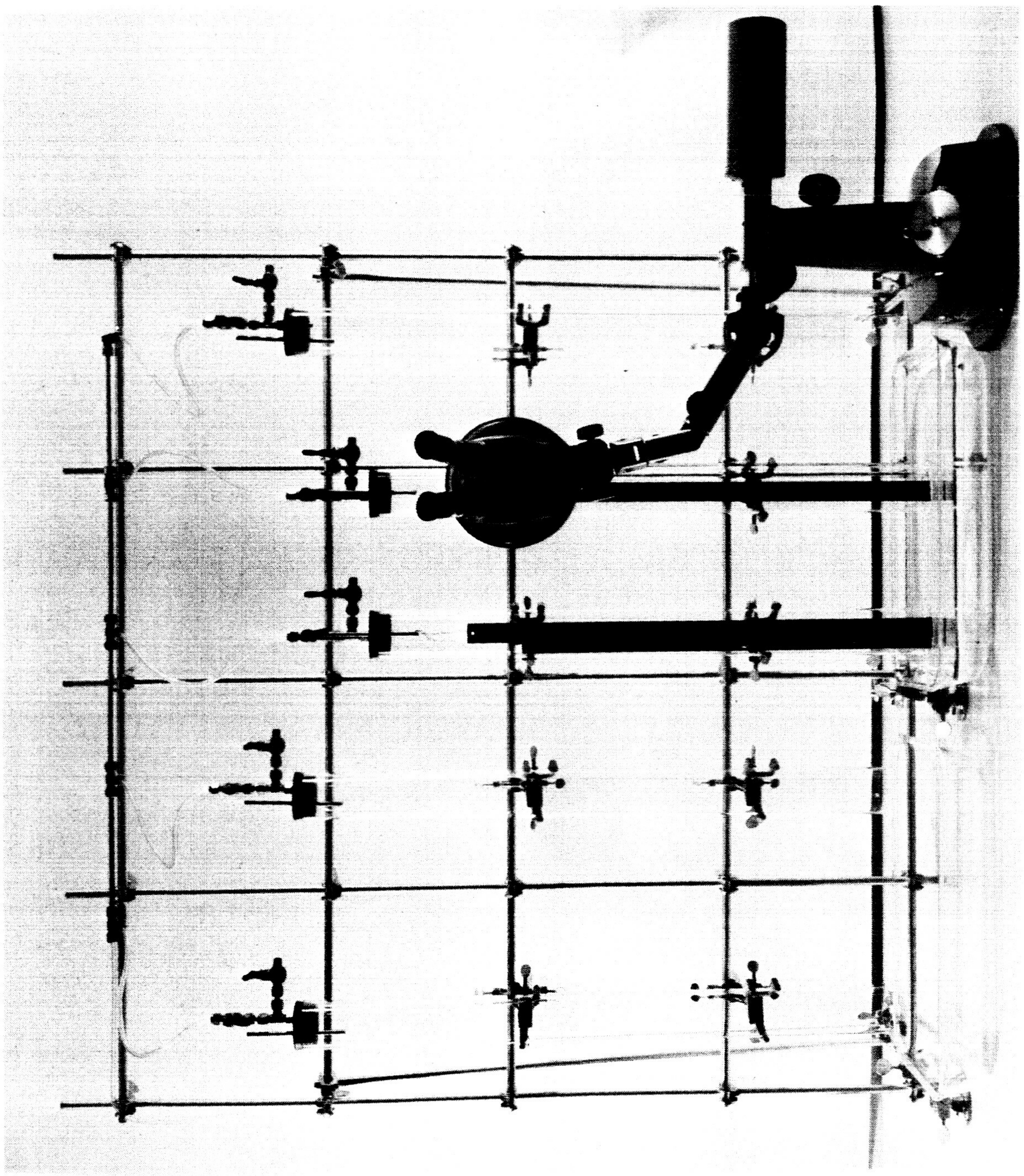

Figure 18 Photograph of Wicking Rise Apparatus. Wicking Material Samples are Suspended Inside Glass Tubes. Microscope Used for Observing Liquid in Wick

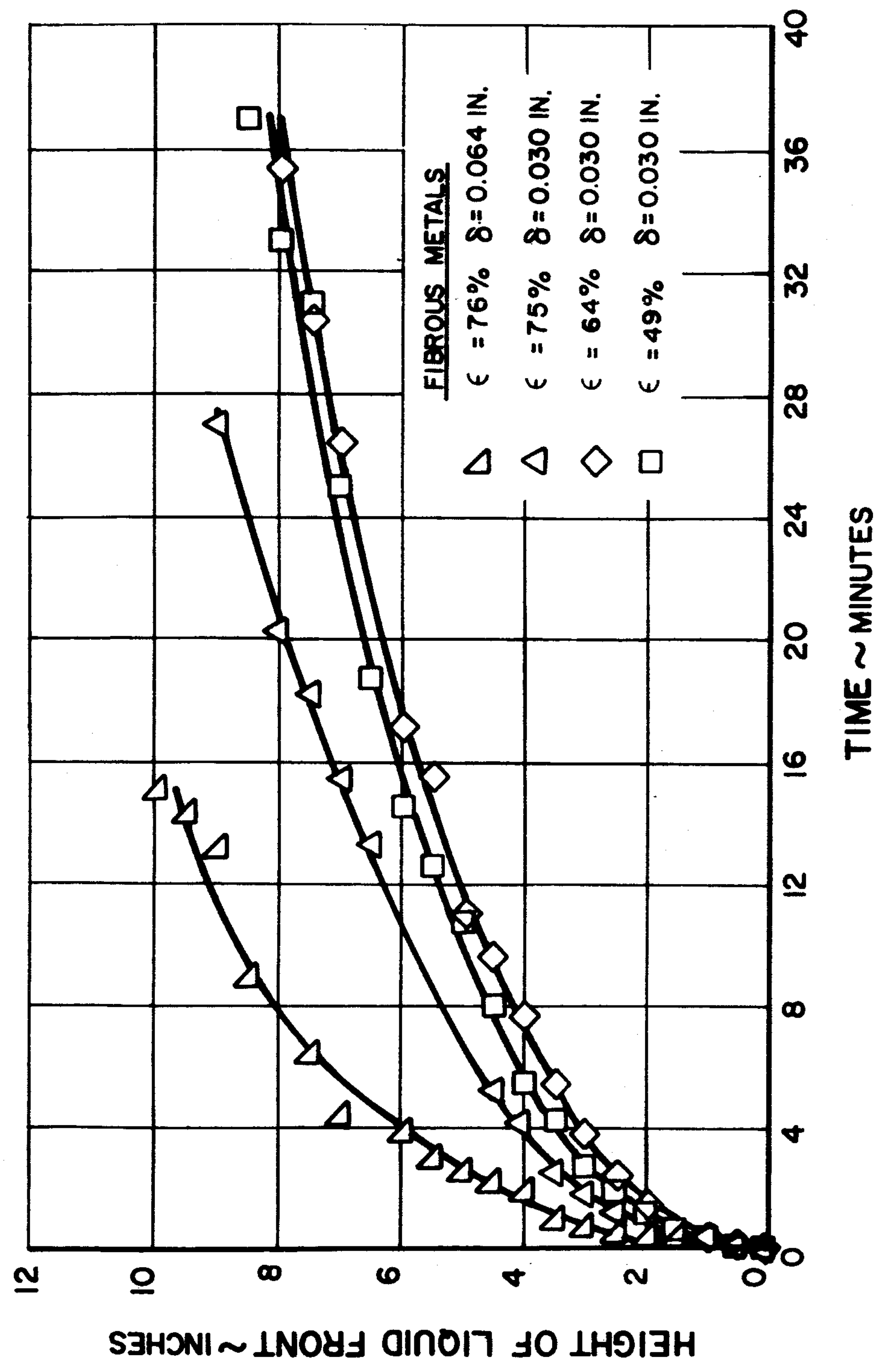

Figure 19 Wicking Curves for Preliminary Fibrous Metal Samples

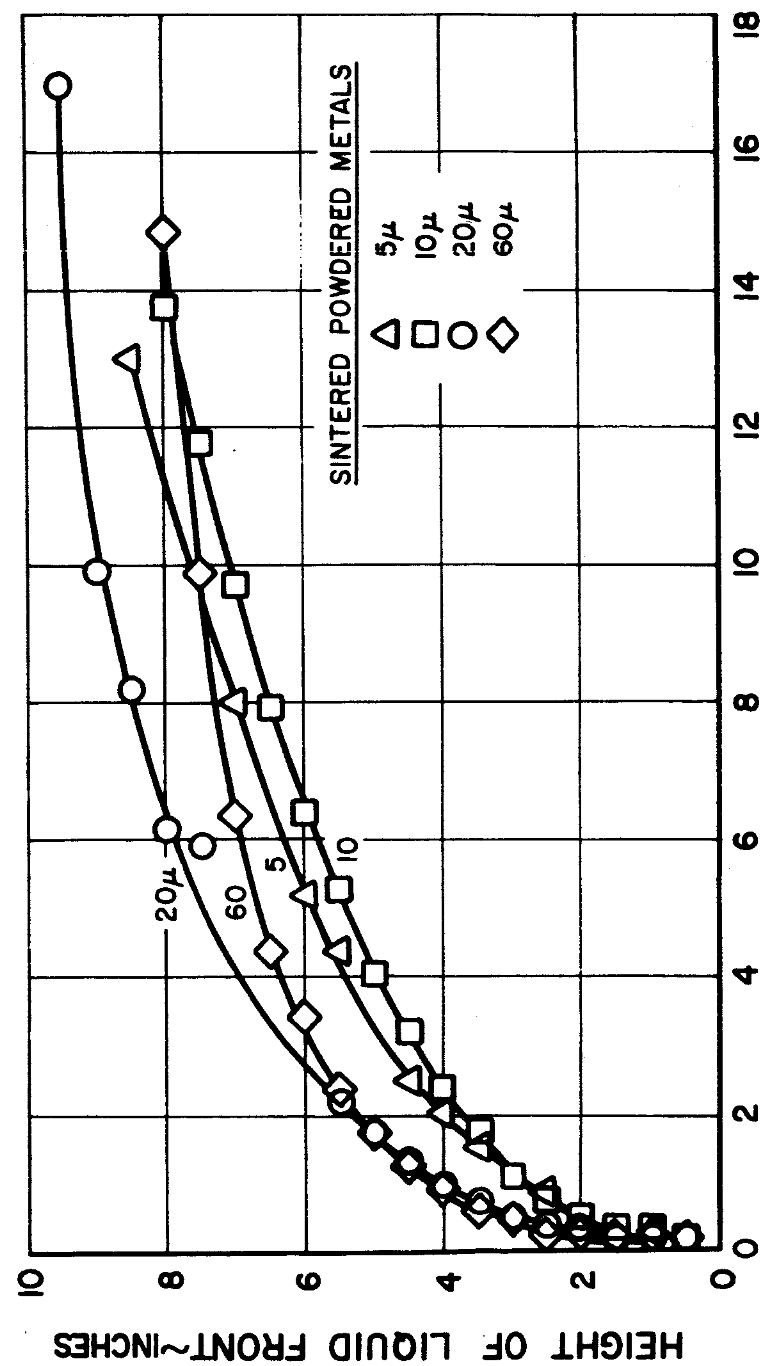

Figure 20 Wicking Curves for Preliminary Sintered Powdered Metal Samples

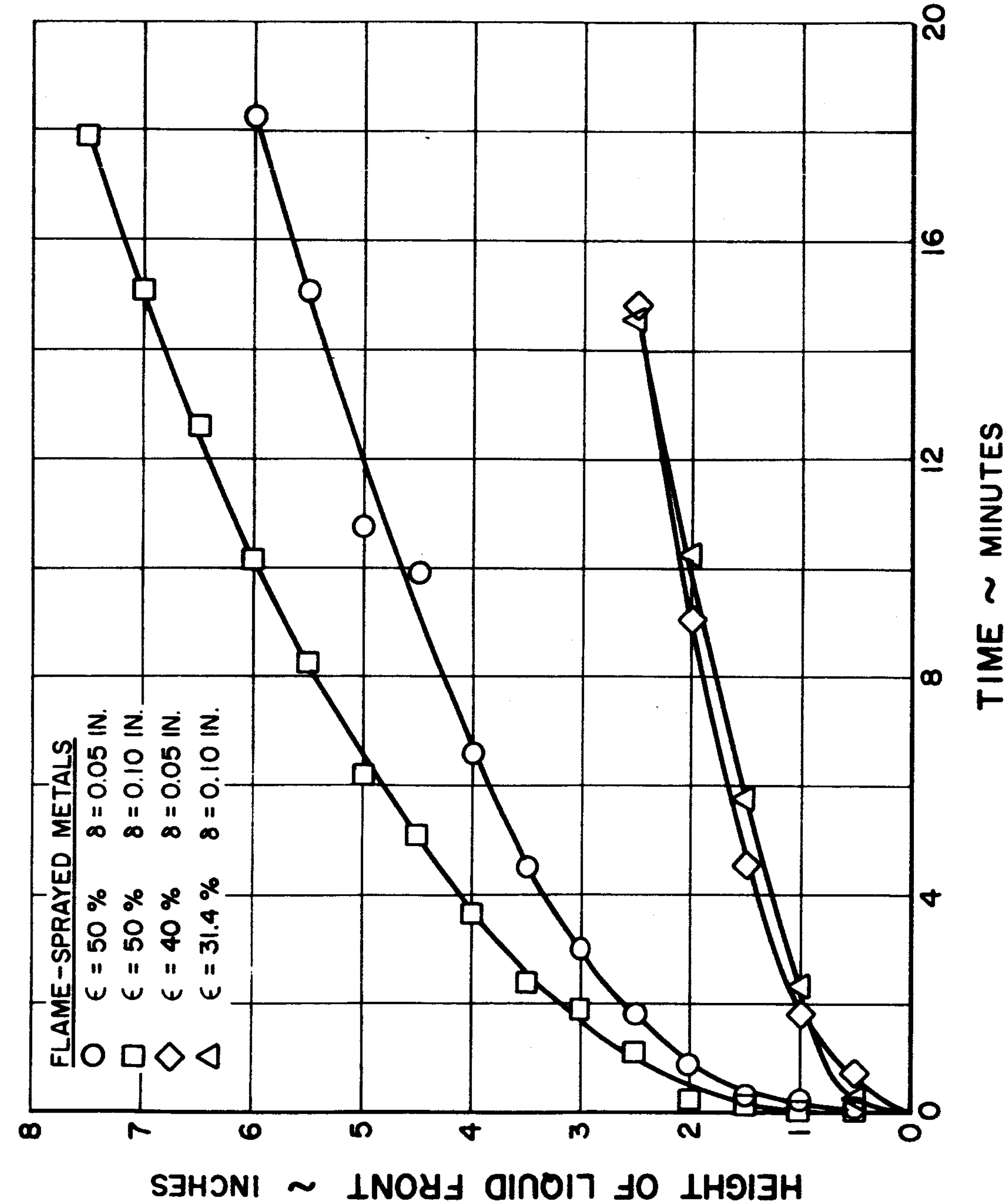

Figure 21 Wicking Curves for Preliminary Flame-Sprayed Powdered-Metal Samples

Wicking curves obtained from the preliminary samples are shown in Figures 19, 20, and 21. Most of the samples represented in these plots were too short to obtain a true ℓ_m. Because of this, no interpretation will be made of these data at this time.

In Figure 19, ϵ is the porosity of each sample and δ is the wick thickness. In all cases the material is nickel fiber, with a mean fiber diameter of 0.0008 inch.

The micron rating referred to in Figure 20 is a measure of diameter of the smallest particle that the porous material could filter out of a liquid flow. The porous material is sintered stainless steel powder with a porosity of about 45 per cent.

The material used to get the plots in Figure 21 is a flame-sprayed nickle powder. Again, ϵ is the porosity of each sample and δ is the wick thickness.

To obtain repeatable results it was found that each sample had to be cleaned carefully and handled in such a way as to minimize the danger of surface contamination. Samples were first soaked several times in acetone and distilled water and then placed in a vapor degreasing apparatus. In the latter, fresh benzene vapor is condensed on the sample and allowed to run off. Following this, each sample was thoroughly rinsed in distilled water and placed in an oven at 800 to 1000°F for 1 to 2 hours. This cleaning procedure seemed to eliminate any surface contamination of the wicking material samples. This was judged by noting the ease with which a drop of water would wet the material before and after cleaning.

As soon as the final wicking material samples are received from suppliers, wicking tests to determine ℓ_m will begin.

In the meantime, rate of rise curves will continue to be taken as additional preliminary samples are procured from suppliers.

VI. BOILING STUDIES-TASK 2

A. Boiling in Wicks

The limitation on fin operation due to boiling occurring in the evaporator wick was discussed in Section III.B. It was concluded that a separate test program would be needed to study the process of evaporation and boiling of a liquid in a wick.

A number of investigators have studied boiling at wick covered surfaces, but none of their researches are directly applicable to the heat transfer process in the evaporator section of the vapor-chamber fin. Allingham and McEntire[8] obtained boiling coefficients for a tube embedded in water-saturated ceramic fiber wicking material. However, because their data was taken at relatively low temperatures (120-160°F) and low heat fluxes (1000 - 10,000 Btu/hr ft^2) no conclusion can be drawn about peak heat fluxes. Maximum heat flux data for a wick covered surface was obtained by Costello and Redeker[9], but because of the path taken by the vapor generated at their heater surface, little correlation can be made between their experimental model and the evaporator of the vapor-chamber fin.

The later work of Costello and Frea[10] is perhaps the most germane to the problem of boiling in the fin. By wrapping a cylindrical electric heater in wicking material they were able to obtain pool boiling burnout heat fluxes of as high as 1.2×10^6 Btu/hr ft^2 in water, with a 50°F difference between the heater temperature and the saturation temperature of the liquid. However, the vapor produced was not vented through the wicking material but rose through an opening in the wick above the heater. Thus, the question of the ability of the wick to support the flow of vapor from and liquid to a region of the heated surface was not conclusively answered, because the data of Costello and Frea is both gravity-dependent and geometry-dependent. However, the extremely high value of the burnout flux obtained in their studies is very encouraging.

In view of the lack of information about the heat-transfer characteristics of saturated wicks, the primary objectives of the boiling tests presented here will be to:

1) measure the maximum heat fluxes that a saturated wick-covered surface can sustain before film-boiling sets in, and
2) find how these limiting heat fluxes vary with wick thickness and between wicking materials.

Both test fluids will be used in some tests. The effects of different orientations with respect to gravity will also be investigated.

B. Description of Boiling Apparatus

A sketch of the boiling test rig is shown in Figure 22, and a photograph of the primary tank with Plexiglas cover is shown in Figure 23. The rig includes a Textolite test platform mounted in a stainless steel primary tank. Two magnesium oxide blocks, with a nichrome guard heater sandwiched between, rest on top of the platform, while two copper busbars are attached to the platform sides. Brazed to the top surfaces of the busbars is a strip of Inconel X750, which heats the wick sample when an electrical current is passed through the Inconel. A strip of mica insulation ($\sim$ 0.0003 inch thick) separates the current-carrying heater from the sample. The Plexiglas cover and neoprene gasket are used to prevent spillage in the tests in which the primary tank is tilted.

The wicking sample consists of a piece 2.875 x 0.625 inch of one of the porous materials listed in Section IV.A. The porous material is bonded to a stainless steel backup plate as shown in Figures 22 and 25. Due to the small size of the sample there is little resistance to fluid flow in the wick. Hence the limiting factor in the determination of the maximum possible heat flux through the wick should be the onset of film-boiling rather than the gross wicking ability of the sample.

The busbar adjusting screws are tightened to press the sample firmly against the mica and heater, thus reducing the overall contact resistance between the heater, mica, and sample, and assuring more uniform heat flux to the liquid-wick-solid interface. This adjustment can be made outside the primary tank as the rig heats up, thereby correcting for thermal expansion of the busbars and heater assembly in the vertical direction.

Thermal expansion of the ceramic blocks and heater in the horizontal direction is allowed for by the elasticity of the busbars in that direction, since the busbars are loosely attached to the sides of the Textolite platform. Also, because magnesium oxide blocks have a coefficient of thermal expansion equal to that of Inconel X750, the resisting force of the busbars will be distributed both in the blocks and the heater. This, coupled with the low resisting force of the busbar, should prevent buckling of the heater due to thermal expansion.

The overall test setup is shown in Figure 24. A stainless steel tank 3.5 x 2 x 0.5 ft is attached to the primary tank. The purpose of the secondary tank is to provide a large liquid-vapor surface, so that the change in liquid height with time as the primary tank fluid is boiled away, is limited to negligible value. In this way, the degree of wick saturation is kept constant during a test. A heater is provided in the secondary tank to keep liquid at a near-saturated condition. A fixture

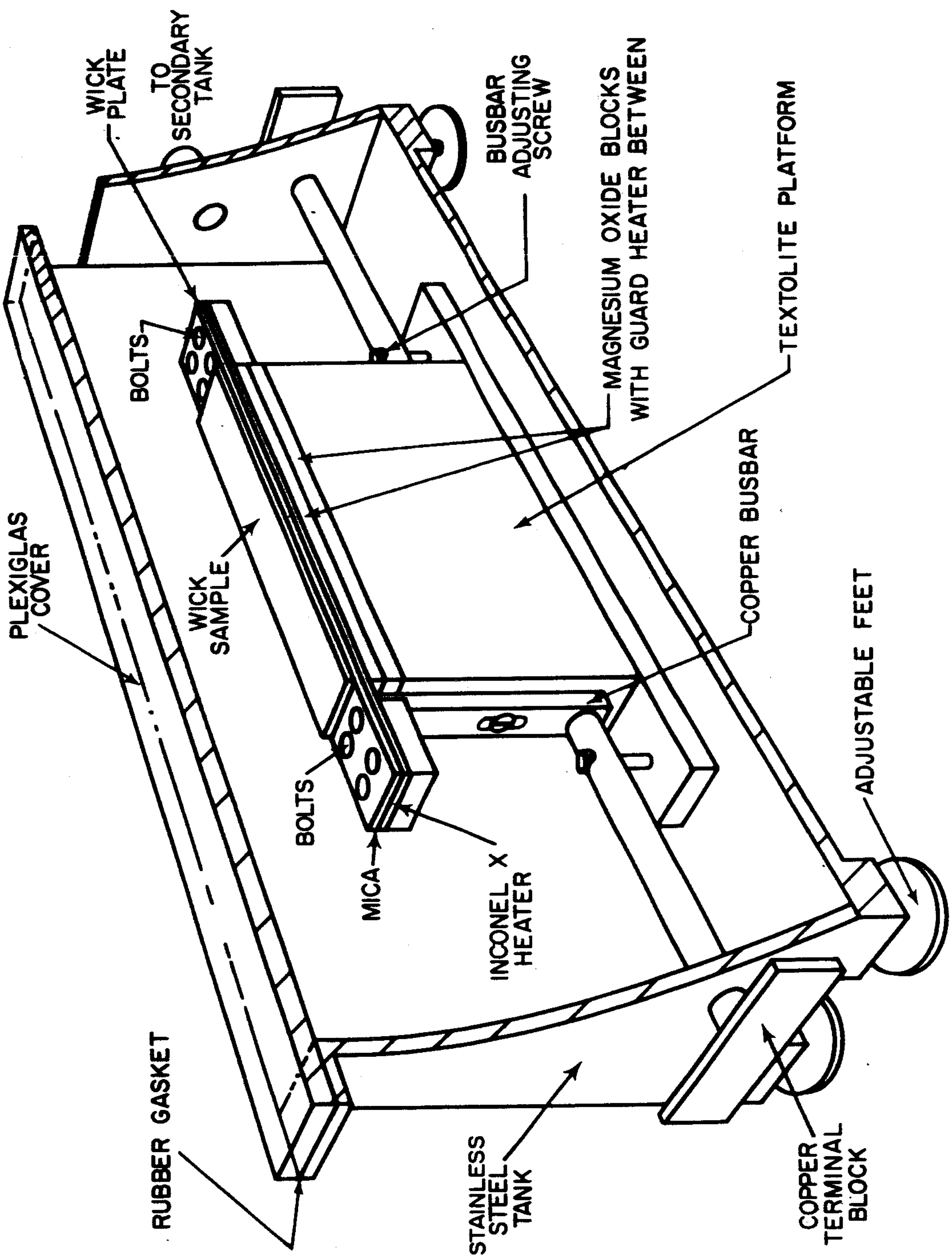

Figure 22 Cutaway View of Boiling Test Apparatus

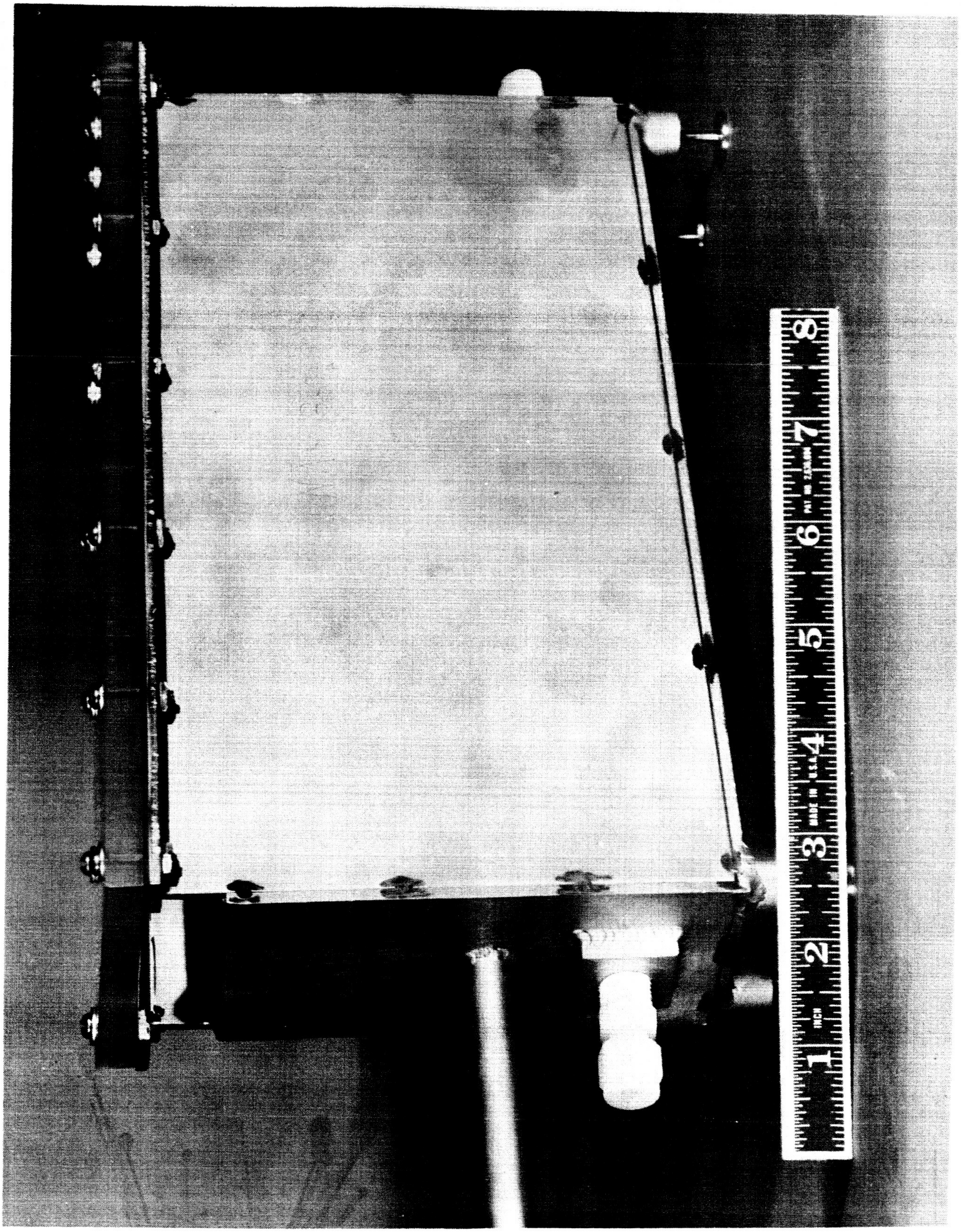

Figure 23 Photograph of Primary Tank of Boiling Apparatus with Plexiglas Cover in Place

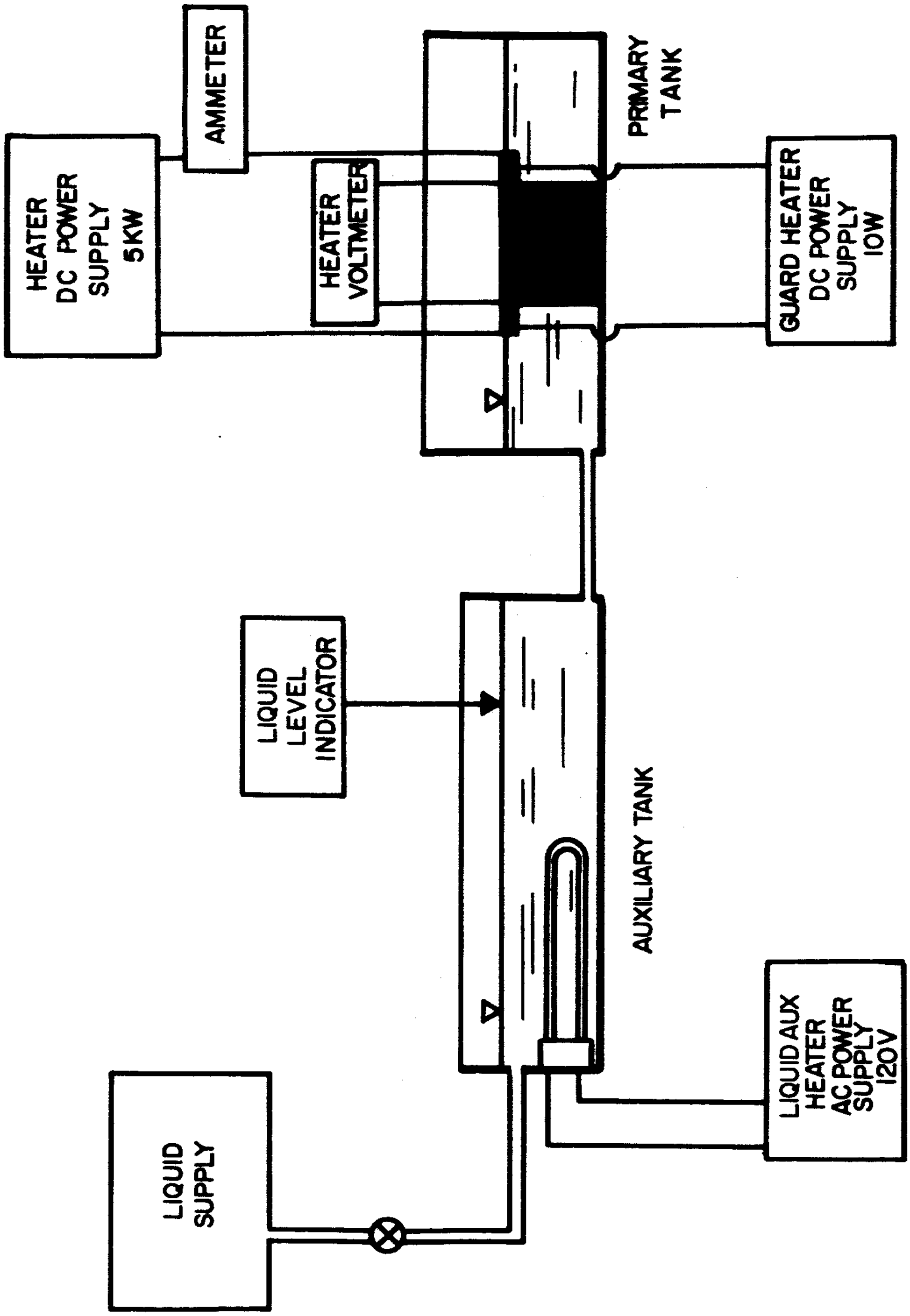

Figure 24 Schematic Diagram of Boiling Test Setup

will be provided to tilt the whole primary tank for non-horizontal tests. The Plexiglas cover with neoprene gaskets is also employed for these tests. Vapor will escape through the port provided in the primary tank. During operation, the production of vapor in the region of the wicking sample should exclude air.

The electrical power inputs to the test rig are shown in Figure 24. Power for the boiling rig heater is supplied by a 12 KVA rectifier with a three-phase 480-volt input and a controllable DC output of up to 750 amperes with 12 volts, or 1500 amperes with 6 volts. The DC output can be controlled in steps of 0.04 volt.

The guard heater power is controlled by two AC 115-volt input powerstats in series. The secondary tank heater is a 5 KW 230-volt resistance type, controlled by a powerstat.

C. Design Conditions

The boiling test apparatus is designed to produce heat fluxes from 0 to 500,000 Btu/hr ft^2. It is possible however that heat fluxes of as high as 1,000,000 Btu/hr ft^2 could be obtained with the apparatus as it is now constructed. The following is a list that summarizes the design condition at a heat flux of 500,000 Btu/hr ft^2 with water:

total heat transfer from heater	6230 Btu/hr
heater current	636 amps
heater voltage drop	3 volts
heater temperature (ceramic block side)	550°F
estimated total heat losses	140 Btu/hr
water level drop rate (without water addition to secondary tank)	0.0029 in/min

The heat losses listed are those that would occur from the heater assembly surfaces which are not guarded or covered by the wicking material.

D. Instrumentation

In all boiling tests two quantities will be determined: q, the resultant heat flux through the wicking sample, and ΔT_{sat} the temperature difference between the saturated vapor and the liquid-wick-solid surface. The heater input is varied so that a plot of ΔT_{sat} vs q is obtained, as shown in Figure 4.

There are six thermocouples in the backup plate of the wicking sample, as shown in Figure 25. These thermocouples serve to determine ΔT_{sat} and to indicate the onset of film-boiling. They are located on the under-

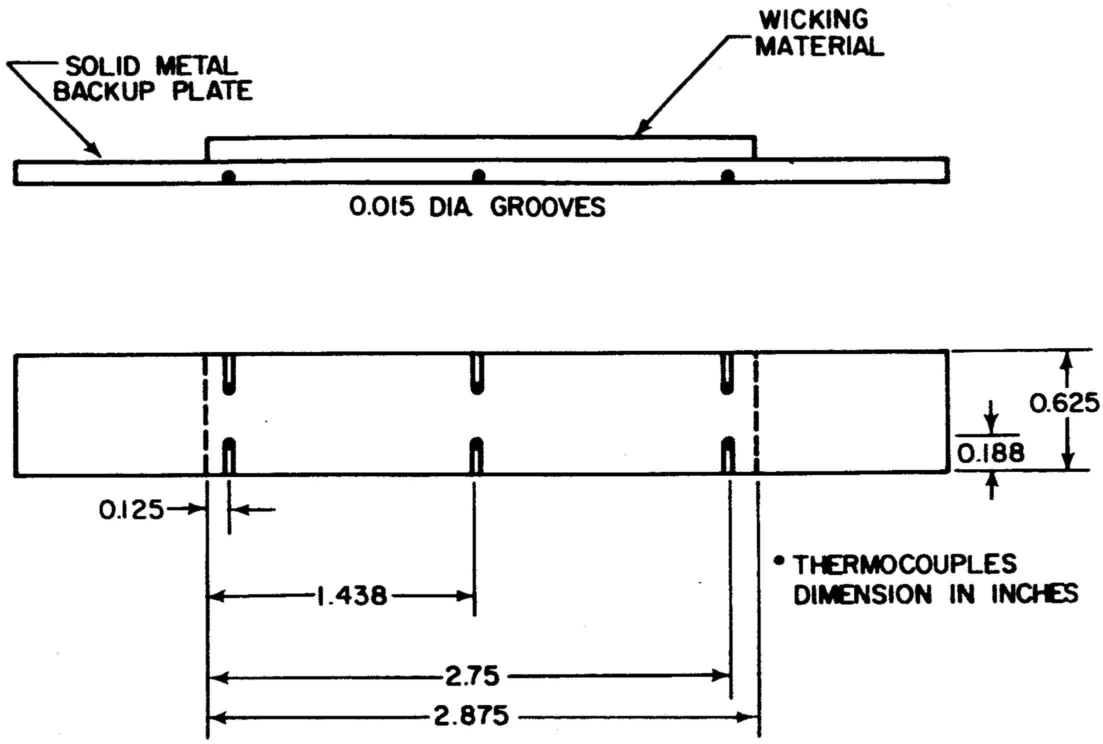

Figure 25 Location of Thermocouples in Boiling Test Specimen

side of the wicking material backup plate, so that the liquid-wick-solid interface temperature is given by

$$T_{\ell ws} = T_B - \frac{Q_B (\Delta x)_B}{A_B \; k_B} \tag{70}$$

where:

T_B = temperature of thermocouple junction

Q_B = heat input to sample
A_B = heater area normal to heat flow
$(\Delta x)_B$ = distance between thermocouple junction and liquid-wick-solid interface
k_B = backup plate thermal conductivity

The thermocouples are not located directly on the liquid-wick-solid interface because of the difficulty in the fabrication of such a design, and because of the possible interference of the wick liquid flow by the thermocouples. Table 3 presents a complete summary of all the instrumentation used in the boiling tests. From Table 3 the maximum error in measuring the total heat transfer at 500,000 Btu/hr ft^2 is about 0.5 watt out of 1908 watts. This combined with the upper limit on heater losses of 140 Btu/hr listed in Section VI. C. makes the maximum uncertainty in q about 2.3 per cent. This value can be made lower if necessary by closely calculating the heat losses from the edges of the heater assembly and accounting for them. The uncertainty in determining ΔT_{sat} can be made small by measuring the differential temperature between the vapor and the backup plate. The uncertainty in the latter reading is about 1 per cent. This coupled with the uncertainty in q yields a maximum experimental uncertainty in ΔT_{sat} of about 10 to 15 per cent. Again, this can be lowered by more closely accounting for heater edge losses.

E. General Boiling Test Procedure

For horizontal tests, the wick will initially be saturated to a selected degree with near boiling fluid from the secondary tank. A particular heat flux will then be imposed with the fluid inlet to the secondary tank set to compensate for the fluid being boiled away (manual adjustments can be made during the tests, if necessary). It is important that the liquid level remain nearly constant in the horizontal tests because a small drop in the level could change the degree of wick saturation. The large surface area of the secondary tank together with manual liquid addition during a test should eliminate this problem.

During the tests, the guard heater will be adjusted to give the same readings for the four thermocouples in the ceramic blocks. This insures that there is zero heat loss on the back surface of the wick heater. At the onset of film-boiling, the sample plate thermocouples will show a sudden rise in temperature. If no film-boiling occurs, instrument readings will be recorded, and a higher heat flux will then be set.

Tests with the primary tank tilted will be run in the same manner as the horizontal, with the following two exceptions:

1) The Plexiglas cover will be used to prevent spillage, and

2) The secondary tank will not be needed once the liquid nearly reaches its boiling temperature, since the decrease in the

TABLE 3

Summary of Boiling Test Instrumentation

Instrument	Quantity	Location and Use	Range of Measurement	Accuracy
thermocouple*	6	Bottom side of wick plate. Used to sense onset of film-boiling, and determine ΔT_{sat}	300 - 350°F	±3°F
thermocouple*	4	Two on either side of top ceramic block. Used to adjust guard heater	300 - 500°F 70 - 300°F	±3°F ±1 to ±3°F
thermocouple*	2	Just below liquid surface approximately 1/2 inch from sample. Used to measure liquid temperature in primary tank	200 - 220°F	±2°F
thermocouple*	2	Approximately 1/2 inch above sample. Used to measure vapor temperature, and determine ΔT_{sat}.	200 - 220°F	±2°F
thermocouple*	2	Immersed in secondary tank near bottom to measure liquid temperature in secondary tank.	200 - 220°F	±2°F
voltmeter	1	Placed across heater to measure voltage drop for heat flux computation	0.5-4 volts	± 0.03 volt
ammeter	1	In series with heater to measure current for heat flux computation	75-600 amps	±5 amps

* all thermocouples are chromel-alumel

liquid level of the primary tank is of little significance when the tank is tilted.

F. Test Progress

The boiling test apparatus has been designed and all parts and power equipment have been procured. At present, the rig is being assembled.

VII. FUTURE WORK

A. Task 1 - Wicking Studies

During the next quarter preliminary testing of wicking samples will continue, by evaluating them on the basis of rate-of-rise curves.

As soon as final wick samples are received from vendors, the wicking rise tests to determine ℓ_m will be started. Each sample so evaluated will then be cut and machined into pieces suitable for testing in both the permeability and the boiling apparatus. In this way uniformity of specimens for each separate test will be assured.

The permeability of each wicking material sample will then be measured, as described in Sections V.A to V.E. The equivalent pore diameter will be calculated using the permeability data and measurements of the porosity. On the more promising samples, pore size distribution, equivalent pore diameter, and the mean pore radius will be determined.

In all of the above studies both data interpretation and analytical work will be carried out in support of the experimental test program.

B. Task 2 - Boiling Studies

As soon as final wicking material samples are received and ℓ_m is measured, boiling tests will begin. In the meantime, to check out the boiling apparatus, pool boiling data for a flat metal strip will be taken. Analytical work will be carried out in conjunction with the boiling experimental work. Emphasis will be placed on obtaining correlating parameters during data interpretation.

C. Tasks 3 and 4 - Fin Studies

Analysis and design of the experimental vapor-chamber fin models to be tested will begin during the next quarter. The results of both the boiling and the wicking studies will give valuable information as to what form these models will take. For instance, if the boiling studies show that extremely high burnout heat fluxes can be attained in wicks, more emphasis in the fin model designs will be placed on the capillary pump and the condenser section. Fin model construction will start during the third quarter.

APPENDIX 1

Nomenclature

APPENDIX 1

Nomenclature

Latin-Letter Symbols

A_B	area of backup plate normal to heat flow
A_c	total cross-sectional area of wick sample normal to liquid flow
b	length of vapor-chamber fin element in z-direction
C_L	specific heat of an incompressible liquid
D_c	equivalent diameter, as defined in Section IV. A.
F	force
F_{AR}	free flow area ratio, defined in Section IV. A.
F_f	force due to friction
g	local acceleration of gravity
g_o	proportionality constant in Newton's second law
h	enthalpy
h_{VL}	latent heat of vaporization
K_1	wick friction factor, defined by Equations (24) or (49)
k	thermal conductivity
ℓ_m	maximum height to which a liquid will rise in a vertical wick sample
M	momentum flux
N	dimensional liquid parameter, $\frac{\rho_L h_{VL} \sigma}{\mu_L}$
P	pressure
P_a	atmospheric pressure
Q	energy per unit time
Q_{crit}	energy per unit time at which fin performance falls off
Q_T	total heat input to a fin
q	heat flux per unit time
R	radius of curvature of a liquid-vapor interface
R_{min}	minimum radius of curvature at the liquid-vapor interface that a given wicking material will support
R_c	radius of curvature of the liquid-vapor interface in pore C
r	pore radius
$\bar{r}$	mean pore radius
T	temperature
$T_{\ell ws}$	liquid-wick-solid interface temperature
u	velocity
u_ϵ	average liquid flow pore velocity
V	volume of pores

w	mass flow rate
x	rectilinear coordinate in x-direction
x_H	total length of a one-dimensional vapor-chamber fin
x_m	total length of the heat-rejecting portion of a one-dimensional vapor-chamber fin
y	rectilinear coordinate in y-direction
z	rectilinear coordinate in z-direction

Greek-Letter Symbols

$\alpha(r)$	pore size distribution function
ΔP	pressure drop
ΔT_{sat}	temperature difference between saturated vapor and the liquid-wick -solid interface
Δx	wick sample length in flow direction
$(\Delta x)_B$	backup plate thickness
δ	liquid-wick thickness
ϵ	porosity, defined as total void volume divided by total sample volume
θ	liquid-solid contact angle, measured within the liquid
μ	absolute viscosity
ρ	density
σ	liquid-vapor surface tension

Superscripts

k	due to conduction
c	due to convection

Subscripts

B	backup plate
d	friction and inertia
L	liquid
S	solid
V	vapor
VL	vapor-liquid
x	at a given x
$x + dx$	at a given x + dx
σ	surface tension
1	at point 1
2	at point 2

APPENDIX 2

References

APPENDIX 2

References

1. Grover, G. M., T. P. Cotter, and G. F. Erickson, Structures of Very High Thermal Conductance, J. of Appl. Phys., June 1964, 35, p. 1190

2. Deverall, J. E. and J. E. Kemme, High Thermal Conductance Devices Utilizing the Boiling of Lithium or Silver, Report No. LA-3211, April 9, 1965, Los Alamos Scientific Laboratory, Los Alamos, New Mexico

3. Deverall, J. E. and J. E. Kemme, Satellite Heat Pipe, Report No. LA-3278-MS, April 20, 1965, Los Alamos Scientific Laboratory, Los Alamos, New Mexico

4. Haller, H. C., S. Lieblein, and B. G. Lindow, Analysis and Evaluation of a Vapor-Chamber Fin-Tube Radiator for High-Power Rankine Cycles, NASA TN D-2836, June 1964, NASA Lewis Research Center, Cleveland, Ohio

5. Adamson, Arthur W., Physical Chemistry of Surfaces, Interscience, 1960, pp 4-6

6. Scheidegger, Adrian E., The Physics of Flow Through Porous Media, Macmillan, 1960, pp 68-90

7. Ginwala, K., T. A. Blatt, and R. W. Bilger, Engineering Study of Vapor-Cycle Cooling Components for Space Vehicles, Tech. Doc. Repts. No. ASD-TDR-63-582, Sept. 1963, AF Flight Dynamics Laboratory, Air Force Systems Command, Wright-Patterson Air Force Base, Ohio, pp 120-148

8. Allingham, W. D., and J. A. McEntire, Determination of Boiling Film Coefficient for a Heated Horizontal Tube in Water-Saturated Wick Material, J. Heat Transfer, Feb. 1961, pp 71-76

9. Costello, C. P., and E. R. Redeker, Boiling Heat Transfer and Maximum Heat Flux for a Surface with Coolant Supplied by Capillary Wicking, Chem. Engr. Progress Symp. Series, 1963, No. 41, 59, pp 104-113

10. Costello, C. P., and W. J. Frea, The Role of Capillary Wicking and Surface Deposits in the Attainment of High Pool Boiling Burnout Heat Fluxes, AIChE Journal, May 1964, 10, pp 393-368

11. Cotter, T.P., Theory of Heat Pipes, Report No. LA-3246-MS, Los Alamos Scientific Laboratory, Los Alamos, New Mexico

12. Fox, H.W., E.F. Hare, and W. A. Zisman, Wetting Properties of Organic Liquids on High Energy Surfaces, J. Phys. Chem, 1955, 59, p. 1098